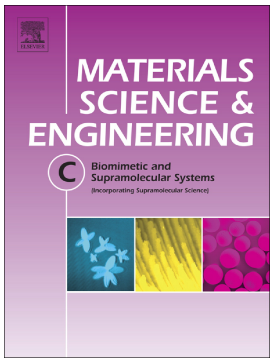

Iron oxide nanoparticles based magnetic luminescent quantum dots (MQDs) synthesis and biomedical/biological applications: a review

Ali Tufani, Anjum Qureshi, Javed H. Niazi

PII: S0928-4931(20)33463-9

DOI: https://doi.org/10.1016/j.msec.2020.111545

Reference: MSC 111545

To appear in: *Materials Science & Engineering C*

Received date: 13 July 2020

Revised date: 11 September 2020

Accepted date: 20 September 2020

Please cite this article as: A. Tufani, A. Qureshi and J.H. Niazi, Iron oxide nanoparticles based magnetic luminescent quantum dots (MQDs) synthesis and biomedical/biological applications: a review, *Materials Science & Engineering C* (2020), https://doi.org/10.1016/j.msec.2020.111545

Iron oxide nanoparticles based magnetic luminescent quantum dots (MQDs) synthesis and biomedical/biological applications: a review

Ali Tufani, Anjum Qureshi* and Javed H. Niazi *

Sabanci University, SUNUM Nanotechnology Research and Application Center, Tuzla 34956, Istanbul, Turkey

*Corresponding authors email: javed@sabanciuniv.edu; anjum@sabanciuniv.edu

Abstract

Combination of quantum dots (QDs) and magnetic nanoparticles (MNPs) as magnetic quantum dots (MQDs) has a broad range of applications as multifunctional nanoscale devices in biological imaging, medical nano-diagnostics and nanomedicine. MQDs derived from iron oxide nanoparticles and QDs possess excellent superparamagnetic and fluorescent properties, respectively making them multifunctional nanoprobes because of their; (a) strong magnetic strength with tunable functionality, such as rapid and simple magnetic separation, (b) intense and stable fluorescence from QDs combined with tunable biological functionality upon QDs' bio-activation, and (c) imaging/visualization by simple ultraviolet light exposure. These excellent features of MQD nanoprobes enable them to be used for magnetic resonance imaging (MRI) as contrast agents, nano-diagnostic systems for Point-of-Care (PoC) disease diagnosis, theranostics nanorobots and in other bio-medical applications. Most of MQDs are derived from iron based MNPs because of their abundancy, superparamagnetic properties, low cost and easy to synthesize. In this review, we present different methods employed for chemical synthesis of MQDs derived from iron oxide MNPs, their major chemical compositions and important parameters, such as precursor compositions, quantum yield and magnetic properties. The review also summarizes the most frequently used MQDs in applications such as bio-imaging, drug delivery, biosensor platforms and finally ends with future prospects and considerations for MQDs in biomedical applications.

Keywords: Magnetic iron oxide nanoparticles; quantum dots; nano-diagnostics; drug delivery; MRI; biological applications

1. Introduction

Combination of fluorescent materials and magnetic nanoparticles (MNPs) find significant importance as multimodal fluorescent-magnetic hybrid nanomaterials mainly in biological applications. These hybrid nanomaterials carry fluorescent and magnetic properties that make them most suitable for *in-vitro* and *in-vivo* biological imaging, medical diagnostics, treatment and drug delivery systems. Until recently, a variety of organic dyes have been used as fluorescent materials in combination with magnetic nanoparticles for biological analysis [1-5]. However, using traditional organic dyes have limitations in their performance due to their pH dependency, photo-bleaching, narrow absorption wavelength, asymmetric emission spectra, small stokes shifts, and short excited state fluorescent lifetime [6-8]. Recently, QD nanocrystals with sizes 2-10 nm has attracted much attention due to their particle size and composition-tunable emission, broad excitation and absorption range, narrow and symmetrical photoemission and strong luminescence and robust photo-stability. These QDs have found applications in biosensors, biological imaging, laser diodes, light devices and energy material because of their unique size dependent physico-chemical and optical properties. QDs are semiconductor nanocrystals composed of groups II–VI or III–V elements and found to be excellent inorganic fluorophores that exhibit luminesce and glow when excited by a specific wavelength light source, offering significant advantages over conventional organic dyes for biomedical and biological applications [9-12].

Semiconductor QDs can be alternative to organic fluorophores in biological applications, where QDs are made of II/VI group elements (such as CdSe, CdTe) that presents inherent cytotoxicity due to individual ions (Cd^{2+}, Se^{2-}, and Te^{2-}). To overcome this issue, a thick shell of ZnS is usually grown over the core CdSe or CdTe nanoparticles making them less toxic as compared to ions of core dots. The outer shell of ZnS serves as a barrier that prevents from contact of core (CdSe) with surrounding solvent and dissolve from ionization. The outer shell also enhances the quantum yield by passivating the non-radiative recombination sites on core surface. Semiconductor QDs based on the elements of groups III–V found to be less toxic and more stable due to the presence of a covalent bond as compared with an ionic bond in the semiconductor QDs element of II-VI group [13]. QDs functionalized with desired affinity ligands or receptors could offer extensive multiplexing when used combinatorially with varying QD sizes and surface ligands/receptors, they not only provide specificity and sensitivity, but also enable bio-imaging, photodynamic therapy and quantitatively measuring the target molecules/pathogens or serum biomarkers. QD-based bio-conjugates were applied into FRET diagnostic probes [14-16], western blotting [17], microbeads labeled-microarrays [18, 19], QD-fluorescence quenching assays [20-22] and other QD-based immunochemistry assays [23-27] for the cancer protein disease biomarker detection [28]. But most of these reported biological systems suffer from colloidal nature of QD dispersions which prone to steric hindrance and less successful owing the physical or chemical stability and insufficient sensitivity in

biological assays. Although, many approaches have been attempted to improve QDs physico-chemical stability [28, 29]. However, fabrication of QDs based bio-conjugation assays for biological application are challenging because QDs cannot be easily functionalized with bio-receptors and shown to have irreversible precipitation and quenching [28, 30].

The MNPs composed of iron oxide (Fe_3O_4) exhibit paramagnetic characteristic in solution and substantially restrict their potential aggregation [31]. These MNPs have been successfully used in magnetic activated cell separations, single molecule manipulation and magnetic resonance imaging (MRI), which is approved by FDA [32]. Utilization of biological receptor functionalized with pure MNPs alone provide easy separation, collection and rapid filtration of the probes, however their applications are limited for rapid qualitative diagnostic test in resource limited settings. MQDs composed of both MNPs and QDs on other hand have found multifunctional nanosystems with collective luminescence and magnetic functionality most desirable in *in vivo* and *in-vitro* bio-imaging and therapeutic applications [33]. Individual QDs or magnetic core-shell nanostructures alone have been extensively used for targeted drug delivery or medicinal applications [reviewed in 34]. In the present paper, we reviewed different synthesis methods for MQDs composed of both iron oxide MNPs and QDs components in a single nanoarchitecture. This review also summarizes the most frequently utilized MQDs in various applications, such as drug delivery, bio-imaging, hyperthermia, magnetic heating, various biosensor platforms and highlighted the major chemical compositions, synthesis parameters such as precursor compositions, quantum yield, magnetic properties and designing of MQDs based bioassay.

This review covered three different chemical methods to synthesizing MQDs mainly by heterocrystalline growth, co-encapsulation or assembly of QDs and magnetic nanoparticles, and doping of QDs with paramagnetic transition metal ions. In the following sections, we describe each of the above MQD synthesis categories in view of their proven biomedical/biological applications.

2. Synthesis of MQDs by heterocrystalline growth

Combination of QDs and MNPs as core-shell or two distinct asymmetric nanoparticles (heterodimer) or dumbbell-like nanoparticles can be synthesized by hetero-crystalline growth method. Lee et al. [35] synthesized colloidal nanostructures combining magnetic FePt with PbS and PbSe in the form of core-shell nanostructures (nanodumbbells) (Figure 1a-b). At first, FePt magnetic nanoparticles were synthesized and then these nanoparticles were dissolved in toluene and injected to lead oleate complex under nitrogen gas flow. The solution of bis(trimethylsilyl)sulfide (TMS_2S) in octadecene was then injected rapidly to form PbS shell around the FePt nanoparticles. The controlled reaction time and temperature of lead oleate complex governed the thickness of PbS shell and shape of core-shell nanoparticles. Injection of TMS_2S solution into lead oleate complex at 100 ºC gave rise to spherical FePt-

PbS core-shell nanostructures (Figure 1a), while at 150 ºC yielded cubic core-shell nanostructures (Figure 1c)). FePt-PbSe nanostructures were synthesized using trioctylphosphine selenide instead of TMS_2S solution. In this method, to synthesize dumbbell-like FePt-PbS nanostructures, FePt magnetic nanoparticles were washed extensively from oleylamine ligands and recapped them with less labile oleate ligands (Figure 1a). These MQDs nanostructures exhibited semiconductor-type transport properties with magnetoresistance and magnetic tunnel junctions. However, Pb based QDs are more suitable for optoelectronic applications due to IR emission characteristics but the presence of Pb pose cytotoxicity threat to living cells and therefore not suitable for biological applications.

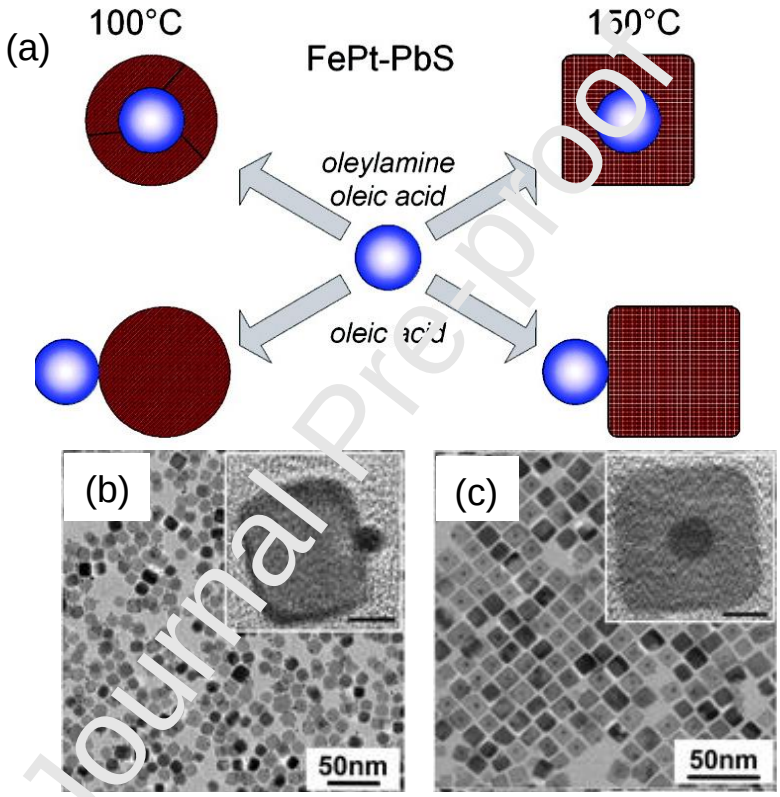

Figure 1. (a) Schematic shows synthesis conditions for FePt-Pbs nanodumbells and cubical core shell or heterodimer morphologies at 100 ºC and 150 ºC, respectively [35]. (b-c) Transmission electron microscopy (TEM) images of FePt−PbS nanostructures with (a) dumbbell and (b) cubic core−shell morphologies [35].

Dumbbell shaped iron phosphide-CdTe (FeP-CdTe) MQDs were synthesized by one pot method [36]. To synthesize multifunctional fluorescent MQDs nanocomposites, first magnetic nanocrystals were formed, and then, without additional purification steps, precursors for QD formation were added to the same reaction flask that yielded heterodimer structures. This method was based on high temperature precursor decomposition in which iron pentacarbonyl solution was injected in hot solution of

trioctylphosphine (TOP) and trioctylphosphine oxide (TOPO) under argon flow to form FeP magnetic nanoparticles. To synthesize nanocomposite of magnetic fluorescent nanocrystals, cadmium oxide and tetradecylphosphonic acid was added to the reactor containing previously synthesized FeP nanoparticle solution. Then, a separately prepared solution of tellurium in TOP was injected in CdO solution to form heterodimer MQDs. These synthesized MQDs displayed paramagnetic property whereas that the free FeP nanoparticles displayed ferromagnetic property. This study suggested that interaction between magnetic and fluorescent properties occur in MQDs which maybe attributed due to alteration of the FeP nanoparticle structure following complexation with CdTe QDs. The high temperature decomposition process facilitated migration of atoms within crystal lattice and resulted in structural rearrangements through doping of FeP nanoparticles or surface adsorption of CdTe phase. Moreover, it is demonstrated that the intensity of photoluminescence (PL) peaks could be tuned by changing the precursor FeP:CdTe ratios to obtain desired optical properties of MQDs [36].

In another report, heterodimer CdSe-γFe_2O_3 MQDs was synthesized by seed mediated high temperature method [37]. Bi-functional MQDs with tunable emission properties were achieved by seed-mediated growth of fluorescent CdSe QDs around γ-Fe_2O_3 magnetic cores at high temperature (300 °C) in the presence of organic surfactants. In seed mediated growth method, first maghemite was synthesized by mixing iron pentacarbonyl, octyl ether and oleic acid and heating this mixture at 280 ºC for 1 h followed by cooling to room temperature. After this, an oxidant was added, and the temperature was raised to 130 ºC and maintained for 2 h. The maghemite nanoparticles formed was cooled to room temperature, precipitated and washed with ethanol and dried. To synthesize MQDs, CdO and stearic acid were heated to 150–200 ºC and then cooled to the room temperature. Maghemite, TOPO and hexadecyl amine (HDA) as the surfactant were added to the mixture and heated to 280–300 ºC. Se solution in trioctylphosphine was quickly injected into the mixture that allowed the QDs to grow at different time intervals to yield different sizes of QDs. Finally, MQDs thus synthesized were precipitated and separated by a magnet and dried. These MQDs were then coated with a thin silica layer via the reverse microemulsion method in order to functionalize with polyethylene glycol (PEG). For this, MQDs was dispersed in chloroform and then aminopropyl trimethoxysilane (APS) was added to the solution and stirred for 1 h. Then, tetramethyl ammoniumhydroxide (TMAH) in 2-propanol/methanol was added to the mixture. After 1 h of stirring, deionized water was added and continued stirring to form MQD-SiO_2 nanoparticles. The nanoparticles were washed with chloroform to remove surfactant and unreacted chemicals. A second APS layer was added to the MQD-SiO_2 dispersed in phosphate buffered saline (PBS) for better dispersity. This method required high temperature to decompose precursor for the fabrication of heterodimer MQDs structure as shown in Figure 2(a-f). Moreover, crystallographic lattice match between MNPs and QDs, reaction temperature and ligand-type in MNPs are some factors that affect surface energy and formation of QDs

around or beside the MNPs. Important issue in heterocrystalline growth, MQDs exhibited very low PL and quantum yield (QY) because of crystal lattice mismatch between MNPs and QDs. Further research experiments are required that should be directed toward preserving the native PL and QY of QDs within MQDs, while keeping its heterodimer structure intact, which will allow to achieve efficient multimodal functionality for biological applications. Further, Lin et al. bioconjugated as-synthesized MQD-SiO_2 nanoparticles and successfully labeled the cell membrane of HepG2 human live cancer cells and 4T1 mouse breast cancer cells (Figure 2g-h). For this, MQDs was activated using oleyl-O-poly (ethyleneglycol)-succinyl-N-hydroxysuccinimidyl ester denoted as bio-anchored membrane (BAM) and the NHS ester was formed with surface amine group on MQD-SiO_2, or by reaction of the surface silanol groups on the silica-coated particles with the aminopropyl trimethoxysilane (APS) conjugated to oleyl-O-poly (ethyleneglycol)-succinyl-N-hydroxysuccinimidyl ester (Figure 2a-f). These functionalized MQDs were used for live HepG2 cell membrane labeling using BAM-functionalized, silica-coated, green and red MQDs as shown the confocal images (Figure 2g-h).

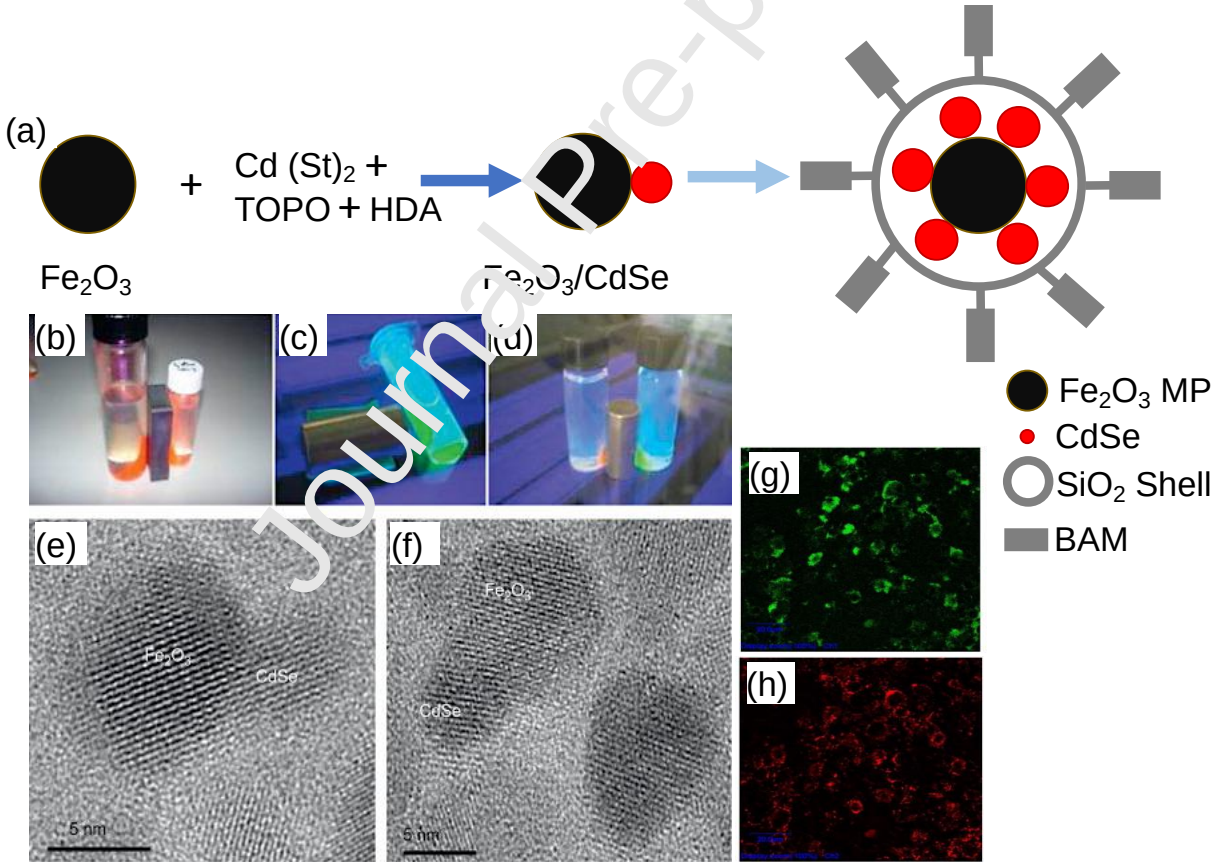

Figure 2. (a) Schematic shows synthesis procedure for heterodimer γ-Fe_2O_3-CdSe MQDs formation and bio-anchored membrane (BAM)-SiO_2-MQDs for bio-labeling, (b–d) photographic images showing the fluorescence and magnetic properties of MQDs after magnetic harvesting and excitation at 365 nm (by UV lamp), and (e, f) HRTEM images of γ-Fe_2O_3–CdSe MQD dimers (11–14 nm) and (g-h): confocal

images of HepG2 live cell membrane labeled using BAM/SiO_2/MQDs with green and red emissions, respectively [37].

Bhandari et al. fabricated new arrangement of superparamagnetic iron oxide nanoparticle (SPION) with ZnS QDs (Fe_3O_4 –ZnS) multimodal nanocomposite, where cysteine-capped quantum dots were grown on the surface of Fe_3O_4 nanoparticles [38]. These nanoparticles were then treated with 8-hydroxy quinoline (HQ) to form octahedral ZnQ_2 complexes on the surface of the ZnS QDs as shown Figure 3a [38]. The new composition (octahedral ZnQ_2) synthesized through complexation reaction of Fe_3O_4–ZnS nanocrystals exhibited high photoluminescence quantum yield, photostability, superparamagnetism, high luminescence stability in human blood serum, non-toxic and magnet guided specific cell imaging properties (Figure 3a-b). This study also demonstrated biological application by utilizing the magnetic property of the MQDs composite for labeling of cells with spatial control using external magnetic field. The SPION Fe_3O_4–ZnS composite exhibited bright green luminescence under confocal microscope using 405 nm diode laser (Figure 3c). The strong green luminescence was observed for the cells incubated with MQDs on the coverslip which was placed near the magnet (Figure 3b), whereas the cells placed away from the magnet showed negligible luminescence. As synthesized SPION Fe_3O_4–ZnS nanocrystals demonstrated possibility to using them for targeted cellular imaging and drug delivery. Table 1 summarizes different precursor compositions, magnetic properties for the synthesis of different types of heterocrystalline MQDs.

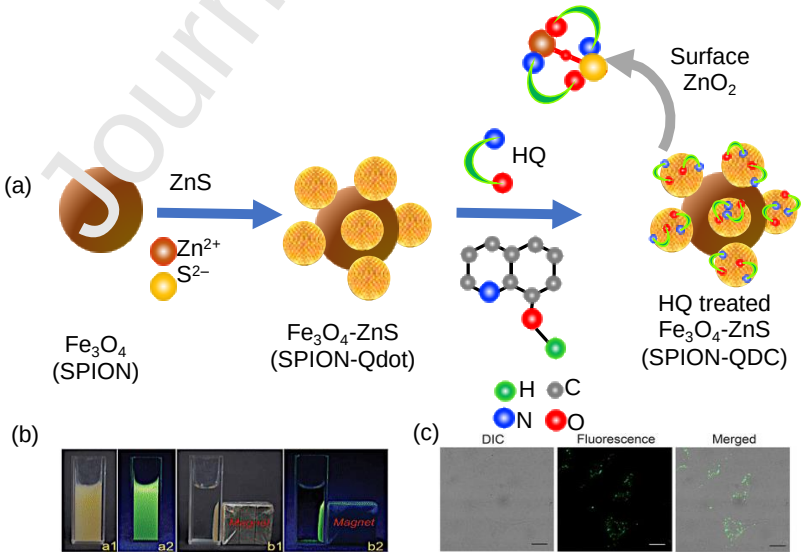

Figure 3. (a) Schematic representation of the formation of Fe_3O_4–ZnS MQDs nanocomposite [38]. (b) Photographs of the aqueous dispersion of Fe_3O_4 –ZnS MQDs nanocomposite in the absence (a1-a2) and presence of an external magnetic field under (b1) white and (b2) UV light (365 nm). (c) Confocal laser

scanning microscopic images (scale bar -25 μm) of cells on slide surface with a magnet placed below coverslip during incubation to pull the cells.

Table 1. Summary and comparison in chemical compositions of different precursors and magnetic properties of synthesized heterocrystalline MQDs.

MNP Precursor	MNP Composition	QD Precursor	QD Composition	MQD Magnetism at (emu g^{-1})	Reference
Platinum acetylacetonate 1, 2-tetradecanediol octyl ether OA; oleylamine; $Fe(CO)_5$	FePt	PbO; OA; ODE; toluene; TMS_2S	PbS	Cubic core-shell: 0.1 Sphere core-shell: 0.075	[35]
		PbO; OA; ODE; toluene; $C_{24}H_{51}Se$	PbSe	Cubic dumbbell 2.1 Sphere dumbbell 1.25 at 300º K	
$Fe(CO)_5$; TOP; TOPO	FeP	CdO TDPA Te powder	CdTe	Paramagnetic property (quantum yield: 25%)	[36]
$Fe(CO)_5$; Octyl ether OA; Trimethylamine N-oxide	γ-Fe_2O_3	CdO; HAD; TOP; TOPO; Se powder; Stearic acid	CdSe	0.3 at 70ºK (quantum yield = 25%)	[37]
Sodium oleate; $FeCl_3.6H_2O$; hexane tetramethylammonium hydroxide; OA; Oleylamine	Fe_3O_4	Cysteine Hydrochloride; Zinc acetate; Na_2S	ZnS	5 (quantum yield = 0.6%)	[38]

3. Synthesis of MQDs by co-encapsulation method

In encapsulation method QDs and magnetic nanoparticles were embedded inside the silica matrix or polymers beads or micelles to fabricate MQDs and the following section describes the most efficient method for co-encapsulation

3.1. Silica coated MQDs

One of the main reasons for coating silica on QDs is because of its biocompatibility and to prevent toxicity, because QDs contain heavy metals that is toxic to living system. Therefore, coating of QDs with biocompatible silica is a suitable method to prevent toxicity effect and to conveniently use them in biological applications. Sun et al. [39] synthesized multifunctional folate-conjugated core/shell silica nanocomposites by encapsulating Fe_3O_4 magnet nanoparticles and CdSeS QDs inside the hollow silica nanospheres fluorescence imaging of cancerous cells. Water soluble cetyltrimethylammonium bromide (CTAB)-stabilized Fe_3O_4 nanoparticles and QDs are used as templates and tetraethylorthosilicate (TEOS)

is used as a precursor to obtain hollow silica nanocomposites as shown in Figure 4a. The magnetic nature of synthesized MQDs nanocomposite was clearly revealed by accumulated intense luminescence with option to simultaneously manipulate using an applied external magnetic field (Figure 4b(i-ii)). Further, this study attempted MQDs conjugation with folic acid as the ligand for interaction with folate receptors in cancer cells, as well as to imaging human cervical carcinoma (HeLa) cancer cells for fluorescence microscopy imaging and analysis.

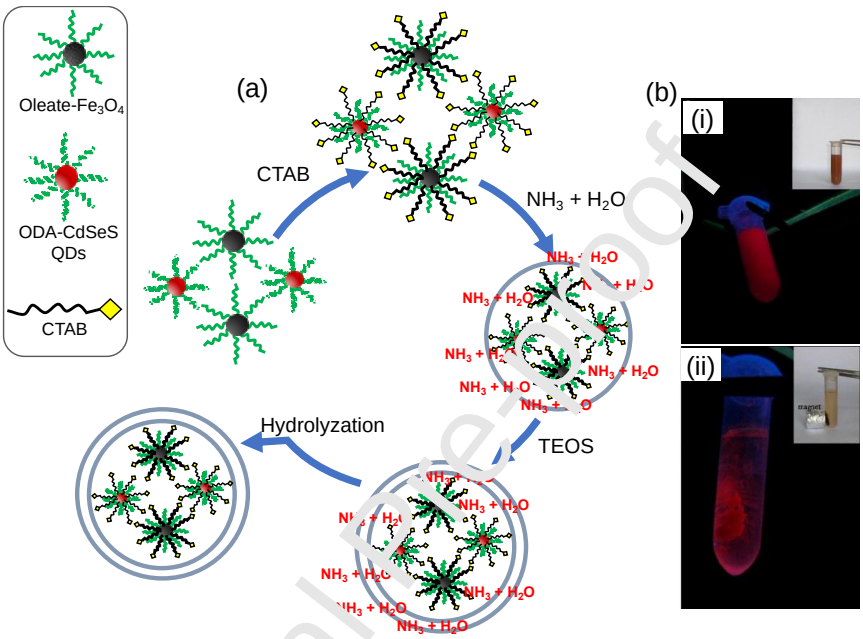

Figure 4. (a) Shows the schem[illegible] for the synthesis procedure of multifunctional folate-conjugated core/shell silica nanocomposites by encapsulated Fe_3O_4 magnet nanoparticles and CdSeS quantum dots inside the hollow silica nanospheres and (b) Photographs of synthesized magnetic and fluorescent silica spheres under natural light and UV irradiation at 365 nm (i) in absence of external magnet field and (ii) presence of external handheld magnetic field [39].

In another study, biocompatible luminescent superparamagnetic Fe_3O_4/SiO_2 cored-CdSe/ZnS QDs were synthesized for radio frequency (RF) treatment of cancer cells. Here, to synthesize Fe_3O_4/SiO_2-CdSe/ZnS MQDs, Fe_3O_4 nanoparticles were coated with a silica shell followed by formation of assembly of water-soluble CdSe−ZnS QDs by the conjugation of an SH group. These MQDs were labeled on cancer cells that were subjected to radio frequency treatment and successfully imaged cancer cells undergoing apoptosis process [40]. Although, these MQDs nanocomposite showed bright orange emission under UV radiation after up-taking into pancreatic human cancer cells, however these nanocomposite particles were relatively large in size. Song et al. [41] embedded Fe_3O_4 nanoparticles and

water soluble CdTe QDs inside silica shell by hydrolysis and condensation of TEOS in presence of ammonia catalyst using reverse micro-emulsion method. This method enabled to synthesize MQDs nanocomposite with different magnetic potential by varying magnetic nanoparticle concentrations during reaction process (Figure 5). The study investigated the capture efficiency of these hybrid nanoparticles using fluorophore-labeled IgG through sequential magnetic separation, capture, and also detection of multiplex antigens using different antibodies under external magnetic field.

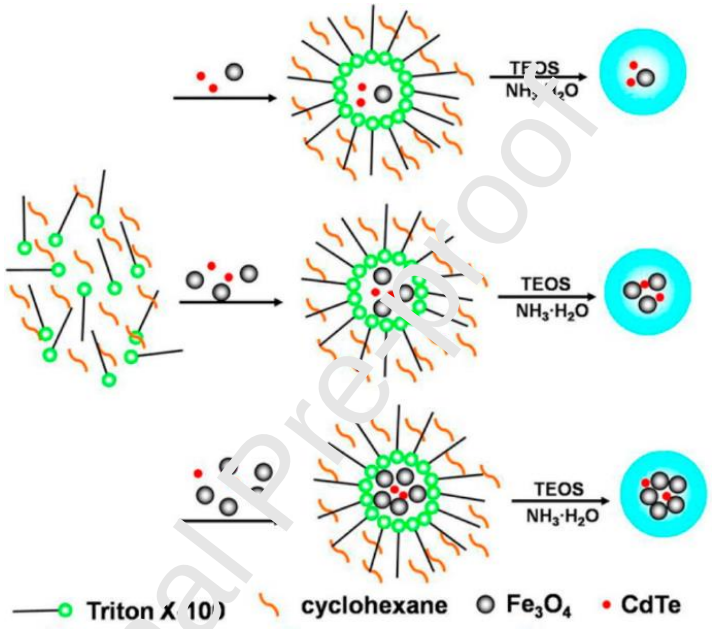

Figure 5. Schematic of fabrication of $(CdTe/Fe_3O_4)@SiO_2$ MQDs with different magnetic potentials [41].

Ma et al. [42] synthesized multilayered core-shell QDs with magnetic nanoparticles for imaging breast cancer tumors. This study reported synthesis of MQDs probes with multimodality imaging capability by the combination of QDs and other functional nanoparticles in the same matrix, which involved MNPs (high T_2 relaxivity), VIS-fluorescent CdSe/ZnS QDs (Em 600 nm), and near infrared (NIR)-fluorescent CdSeTe/CdS QDs (Em 780 nm). For this, a reverse micro-emulsion technique was used in which hydrolysis of TEOS was utilized in the presence of ammonia for Fe_3O_4 nanoparticles/SiO_2 layer formation. Different nanoparticles were encapsulated in the core with a number of silica layers. Then visible-fluorescent CdSe-ZnS QDs (separately prepared) and TEOS were added to the liquid system subsequently condenses to form a thin shell of QDs covered with silica layer and then the hydrolysis of TEOS was utilized to encapsulate NIR CdSeTe/CdS QDs with another layer of silica. (Figure 6a). The multimodality imaging capability of synthesized multilayered MQDs probe was demonstrated by

integrated advantages of MRI, VIS- and NIR-fluorescence imaging techniques using a mouse model for human breast cancer detection (Figure 6b(i-iv)). For this, the surface of nanoparticles was functionalized using 3-aminopropyltrimethoxysilane (APTS), and 3-(trihydroxysilyl)-propylmethyl-phosphonate (THPMP) and bioconjugated anti-HER2 antibody (human epidermal growth factor receptor 2) and BSA via amine and carboxy functional groups. *In-vivo* multimodal near infrared fluorescence imaging of the tumor mice (KPL-4 cells transplanted) was possible due to the property of QDs to excite with near infrared light that had high tissue permeability as shown in Figure 6b(i-iv). It was reported that VIS-fluorescence imaging showed limitation of spatial resolution in *in vivo* imaging due to the strong absorption and scattering by blood and tissues. This problem was solved by integrating NIR CdSeTe/CdS QDs encapsulated with an extra layer of silica. In addition, this work also demonstrated the multimodal *in-vivo* MRI to detect breast tumors more sensitively and accurately using synthesized MQDs exploiting their near infrared fluorescence and magnetic properties.

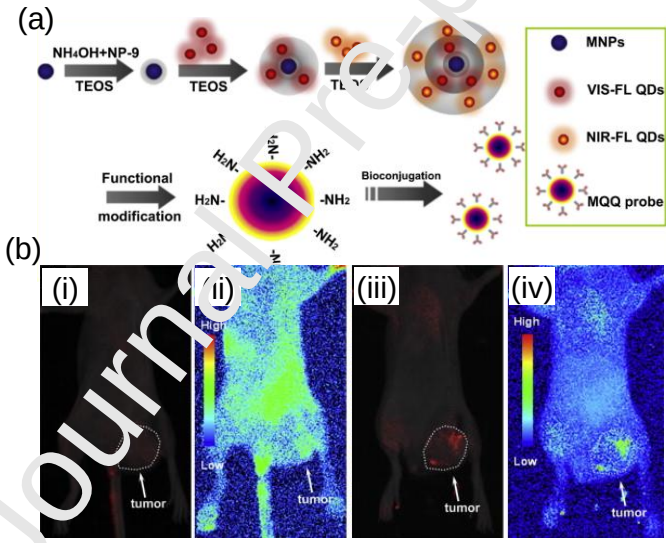

Figure 6. (a) Schematic shows the synthesis process of multilayered core-shell magnetic nanoparticles/silica and QDs probe *via* stepwise encapsulation by micro-emulsion method [42] and (b) *In -vivo* NIR fluorescence imaging of a HER2-MQDs probe injected mice bearing human breast tumors: (i, ii) 0.1 h and (iii, iv) 48 h after injection of the HER2-MQD-probe. The color mapping images of (ii) and (iv) show the fluorescence intensity at 830 nm [42].

Wang et al. [43] synthesized fluorescent magnetic QD nanoparticles composed of silica-wrapped CdTe and Fe_3O_4 magnetic nanoparticles for *in vivo* targeted magnetofluorescent imaging of gastric cancer. These fluorescent magnetic QD nanoparticles were functionalized with free carboxyl groups on

silica-shell surface and conjugated with BRCAA1 monoclonal antibody and *in-vivo* targeted for gastric cancer cells by fluorescence optical imaging and MRI. In another study, fluorescent and superparamagnetic ZnS@Fe_3O_4 nanospheres were synthesized via chemical co-precipitation followed by chemical conjugation [44]. In the first step, (3-mercaptopropyl)trimethoxysilane (MPS) capped ZnS QDs and SiO_2 coated Fe_3O_4 nanoparticles were synthesized separately by using solution growth and co-precipitation techniques. Secondly, ZnS@Fe_3O_4 nanospheres were formed with an average size of around 100 nm by attaching ZnS QDs to the surface of the Fe_3O_4 nanoparticles by Si-O-Si bonds of QDs. The synthesized ZnS@Fe_3O_4 nanospheres exhibited both superparamagnetic and fluorescent behavior [44]. Yin et al. [45] synthesized multifunctional mesoporous magnetic fluorescent nanoprobes, where a surfactant template was used to induce swelling of pores. Mesoporous silica was coated around Fe_3O_4 nanoparticles following layer-by-layer assembly of 3-aminopropyltrimethoxysilane and CdTe QDs on mesoporous Fe_3O_4-silica nanoparticles (Figure 7).

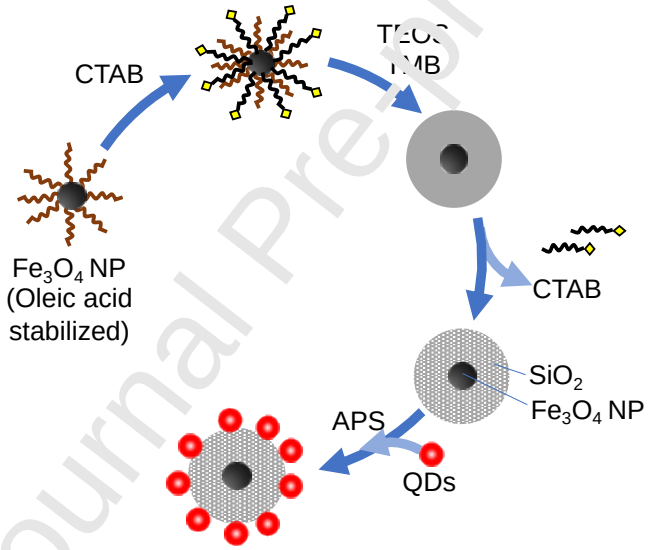

Figure 7. Scheme showing synthesis steps for the preparation of multifunctional mesoporous Fe_3O_4/SiO_2/CdTe nanoprobe using CTAB surfactant template followed by formation of CdTe QDs on Fe_3O_4-silica nanoparticles [45].

Gui et al. [46] synthesized poly(*N*-isopropylacrylamide)-graft-chitosan microgels (PNIPAM-*g*-CS) coated on core Fe_3O_4/QDs dual-embedded in mesoporous silica NPs (MSN) forming multifunctional microspheres with magnetic-fluorescence, thermo/pH-sensitive and drug carrier properties. These Fe_3O_4/CdTe magnetic quantum dot nanocrystals (MQ NCs) were synthesized by electrostatic adsorption with thiodiglycolic acid (TA) stabilized-Fe_3O_4 NPs, polyethylenimine (PEI), and 3-mercaptopropionic acid (MPA)-capped CdTe QDs (Figure 8a step one). Next, MQ NCs were homogeneously encapsulated into silica spheres by modified Stöber method to prepare MQ-MSN (Figure 8a step two). The third step is

divided into two stages, where (i) first *N*-isopropylacrylamide (NIPAM) monomers were initiated PNIPAM networks with MQ-MSN distributed below the lower critical solution temperature (LCST) of PNIPAM. Then, (ii) PNIPAM reacted with CS to form PNIPAM-*g*-CS copolymers above LCST, meanwhile PNIPAM networks collapsed to form hybrid microspheres, resulting in MQ-MSN encapsulated into microspheres (Figure 8I step three). The morphology and structure of synthesized microspheres showed microspheres consisted of black dots (CdTe/Fe_3O_4) encapsulated in the gray interlayer of silica with a dark shell layer with average diameter of 190 ±15 nm in TEM image (Figure 8b). These microspheres were then loaded with a model drug, Adriamycin (ADM) and investigated the effect of temperature and pH on drug release rate (Figure 8I). The ADM-loaded microspheres demonstrated cumulative release of ADM *in vitro* significantly at a higher temperature (or a lower pH) with maintained high anticancer activity, and the blank microsphere carriers hardly produced toxicity to HepG2 cells. This study demonstrated the applicability of MQDs in drug delivery applications.

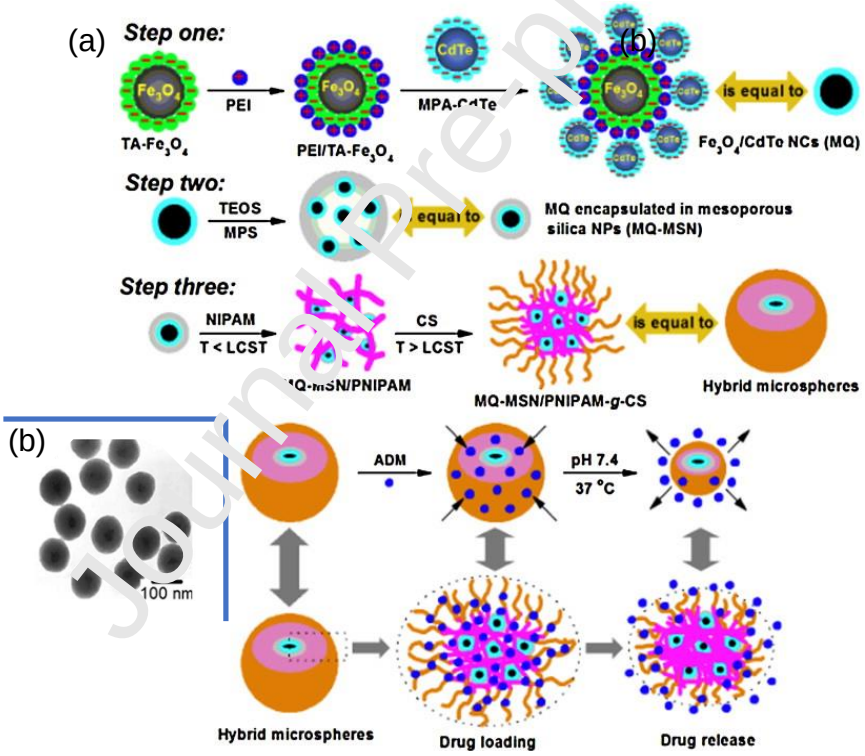

Figure 8. (a) Schematic shows the synthesis procedure of MQ-MSN/PNIPAM-*g*-CS hybrid microspheres in three steps and ADM drug loading and release method. In first step: a base-catalyzed sol–gel method was used in the presence of CdTe QDs and Fe_3O_4 nanoparticles to prepare MQ-MSN NCs, second step: MQ-MSN were dispersed in ethanol containing MPS for surface modification of C-C bonds, which form covalent bonds between inorganic substrates as cores and polymers as shells, step third: using MPS-modified MQ-MSN as seeds, MQ-MSN/PNIPAM-*g*-CS microspheres were prepared by graft

copolymerizing NIPAM and CS. Scheme also illustrate ADM cumulative release *in vitro* from ADM-loaded microspheres at 37 ºC (pH 7.4). (b) TEM image of core/shelled, spherical, and polymer-encapsulated (bright ring) of MQ-MSN/PNIPAM-*g*-CS hybrid microspheres (average diameter of 190 ± 15 nm). TEM image revealed microspheres consisted of black dots (CdTe/Fe_3O_4) encapsulated in the gray interlayer of silica with a dark shell layer (PNIPAM-*g*-CS) [46].

Other studies involving MQDs for drug delivery applications is reported by Knezevic and Lin et al. [47] in which the drug delivery system composed of cored magnetic mesoporous nanoparticles Fe_3O_4-SiO_2 (MMSN) loaded with anticancer drug camptothecin (CPT), while entrances of the mesoporous are blocked with 2-nitro-5-mercaptobenzyl alcohol functionalized CdS nanoparticles through a photocleavable carbamate linkage (Figure 9). This study tested the synthesized drug delivery system for anticancer effects on Chinese hamster ovarian cells. The anticancer effect exerted by the release of drug from the drug delivery system upon exposure to low power UV light (365 nm) is demonstrated. One of the limitation of this system is cytotoxic effect of CdS nanoparticles, which cannot be controlled from synthesized drug delivery system by any stimuli and therefore, toxicity may also be exerted on healthy cells. However, application of magnetic property to drive such drug delivery system to localized drug delivery near the proximity or directly to the cancer tissues and selectivity and enhanced permeability and retention (EPR) effect can thus be achieved [47]. This study demonstrates MQDs as powerful tools for magnetic field assisted selective drug delivery for anticancer therapy which is still largely unexplored.

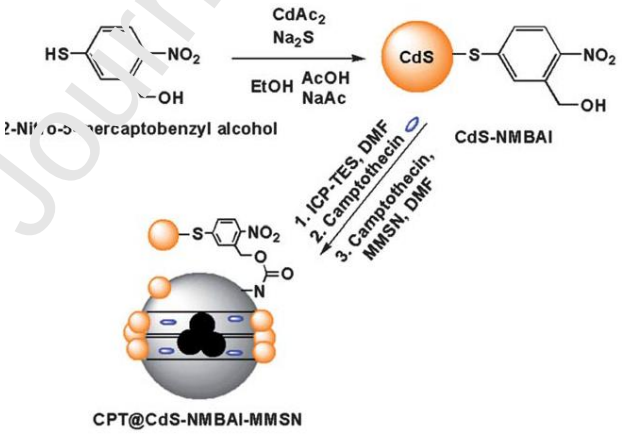

Figure 9. Schematic of functionalization of cadmium–sulfide nanoparticles with 2-nitro-5-mercaptobenzyl alcohol (NMBAl) as CdS-NMBAl. These functionalized QDs used to cap the mesopores of MMSN to camptothecin. ICP-TES = 3-isocyanatopropyl-triethoxysilane inside MMSN [47].

Wang et al. synthesized hydrophilic MQDs made of Fe_3O_4-SiO_2-CdTe for latent fingerprint detection [48]. They coated Fe_3O_4 nanoparticles with silica by reverse micro-emulsion method and the surface was functionalized with (3-aminopropyl) triethoxysilane to generate amine group terminal. CdTe QDs were capped with glutathione (GSH) to create free carboxyl functional surface (Figure 10a). These QDs were later decorated around magnetic nanoparticles forming magnetic-fluorescence nanoparticles via covalent binding between carboxyl and amine groups. This hybrid system showed clear and better quality of latent fingerprint with greater number of detailed features in comparison to pure magnet or QDs (Figure 10b). The bifunctional Fe_3O_4@SiO_2-NH-CO-CdTe- MQDs showed fluorescence imaging for the visualization of latent fingerprints on glass slide as shown in Figure 10b(i-vi). The fingerprint features scanned with synthesized MQDs revealed clear, hook features, and detailed ridged patterns with high resolution most useful in forensic identification related applications.

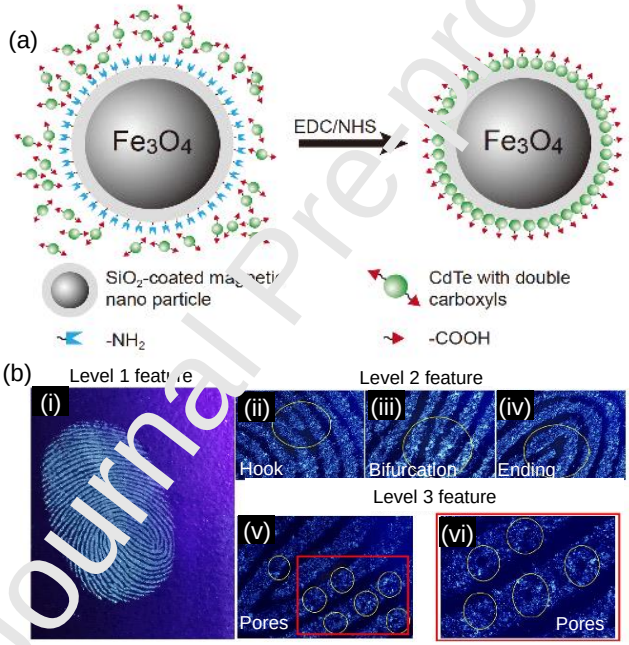

Figure 10. (a) Schematic showing preparation of bifunctional magnetic-fluorescent bifunctional Fe_3O_4@SiO_2-NH-CO-CdTe MQDs. (b) High resolution fluorescence images of features of fingerprints using bifunctional Fe_3O_4@SiO_2-NH-CO-CdTe- MQDs for (i) level 1 clear features of fingerprints, (ii-iv) level 2 features, such as hook, bi furcation and ending and (v-vi) level 3 details feature such as the pores running along the ridged pattern, are helpful to the identification of partial or damaged fingerprints [48].

Qiu et al. synthesized a hybrid of poly(lactic-co-glycolic acid) (PLGA) NPs carrying QDs, SPIONs and Au NPs to utilize each of these nanomaterial properties as one composite multimodal NPs. These multimodal functionality of NPs were exploited in neutrophil labeling, imaging, tracking and manipulating transplanted neutrophils *in vivo* [49]. For fabricating such multimodal NPs, first silica

coated iron oxide NPs and QDs were encapsulated with PLGA by emulsification followed by assembling negatively charged citrate stabilized Au nanoparticles on top of the positively charged PLGA NPs through electrostatic interactions as shown in Figure 11. The uptake of these hybrid PLGA NPs was studied using human neutrophils and the results showed that uptake of PLGA-QD-iron oxide NPs by neutrophils was much higher than the uptake of PLGA-QD-iron oxide-Au nanoparticles. One of the main features, apart from QDs-mediated imaging and tracking of PLGA-QD-iron oxide-Au nanoparticles labeled neutrophils is that they can be sorted and manipulated using magnetic gradient [49].

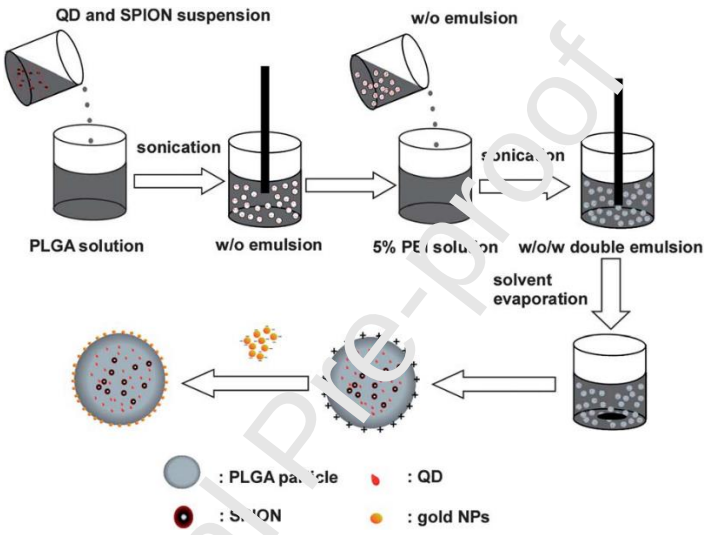

Figure 11. Schematic illustration of the preparation of hybrid multimodal PLGA nanoparticles using water–oil–water (w/o/w) double emulsion solvent evaporation method in which QDs and SPIONs were entrapped in small water drops suspended in the organic phase via sonication. This process is followed by formation of secondary w/o/w emulsion by adding the primary emulsion to a continuous aqueous phase of polyethylenimine (PEI). PEI was used as emulsifying agents stabilizing the organic droplets to form a stable thin layer on the surface of the PLGA particle followed by formation of Au NPs assembly [49].

Hsu et al. synthesized multifunctional agents composed of nanohybrids integrated with $CuInS_2$/ZnS QDs and Fe_3O_4 MNPs for dual-modality imaging and drug delivery applications [50]. These nanohybrids were synthesized by a one-pot two-step reverse microemulsion method. In this method, SiO_2 nanohybrids containing $CuInS_2$/ZnS QDs and Fe_3O_4 MNPs were formed in the w/o microemulsion. These nanohybrids were grafted with PEG that enhances biocompatibility and amine (NH_2) groups for the coupling of Pt(IV)-anticancer drugs to generate cytotoxic Pt(II) through reductive elimination of axial ligands. This study demonstrated that silica based magnetic QD nanohybrids (diameter <30 nm) exhibited dual-

functional (superparamagnetic and fluorescence) properties, exhibited higher cytotoxicity with Pt (IV)-conjugated MQDs in comparison with the free Pt (IV) anticancer drug and high potential to use as a dual-modality imaging probes in cancer diagnosis and chemotherapy applications. Similar MQDs with different compositions have been synthesized for their excellent multi-modal functionalities. Table 2 shows the summary of chemical compositions of different precursors and magnetic properties for the synthesis of silica coated MQDs.

Table 2. Summary and comparison of different chemical composition of precursors and properties of synthesized silica coated MQDs.

MNP's Precursor	MNP's Composition	QDs-Precursor	QDs-Composition	Silica Shell Precursor	MQDs Magnetism (emu g^{-1})	Reference
$FeCl_2.4H_2O$ $FeCl_3.6\ H_2O$ ammonium hydroxide	Fe_3O_4	as- received	CdSeS	CTAB Ammonium hydroxide TEOS		[39]
$FeSO_4.7H_2O$ $FeCl_3.6H_2O$ Ammonium hydroxide	Fe_3O_4	Te powder $NaBH_4$ $CdCl_2.2.5H_2O$ MPA	CdTe	Ammonium hydroxide; TEOS; PDDA; Triton X-100; Cyclohexane; hexane	15 strong 10 medium 2 weak	[41]
As-received	Fe_3O_4	HDA; TOP; TOPO; Se powder; stearic acid; TBP $ZnEt_2$; cadmium 2,4-pentanedionate hexamethyldisilathiane	CdSe/ZnS	Ammonium hydroxide; TEOS; Tergitol; Cyclohexane hexane		[42]
		HDA; TOP; TOPO; Se powder; Te powder; stearic acid; TBP; CdO	CdSe/CdS			
$FeCl_2.4H_2O$ $FeCl_3.6\ H_2O$ NaOH	Fe_3O_4	$Zn(NO_3)_2$ Na_2S MPS	ZnS	Ammonium hydroxide; TEOS	30	[44]
$FeSO_4.7H_2O$ $FeCl_3.6H_2O$ Ammonium hydroxide OA	Fe_3O_4	Te powder $NaBH_4$ $CdCl_2.2.5H_2O$ MPA	CdTe	CTAB Ammonium hydroxide TEOS TMB	7	[45]
$FeSO_4.7H_2O$ $FeCl_3.6H_2O$ NaOH	Fe_3O_4	Te powder $NaBH_4$ $CdCl_2.2.5H_2O$	CdTe	NaOH TEOS Ethyl acetate	6.5	[46]

TA		MPA Thiourea				
$FeSO_4.7H_2O$ $FeCl_3.6H_2O$ Ammonium hydroxide	Fe_3O_4	Cadmium acetate Na_2S Acetic acetate NMBAI	CdS	CTAB TEOS NaOH		[47]
$FeSO_4.7H_2O$ $FeCl_3.6H_2O$ Ammonium hydroxide OA	Fe_3O_4	Te powder $NaBH_4$ $CdCl_2.2.5H_2O$ GSH	CdTe	Ammonium hydroxide TEOS KH-550 MQD quantum yield = 4.25	28	[48]
$FeCl_3.6H_2O$ Sodium oleate Hexane Ethanol OA ODE	Fe_3O_4	As- received		CTAB TEOS NaOH Ethyl acetate		[49]
Iron(iii) Acetylacetonate Benzyl ether oleylamine	Fe_3O_4	Copper acetate; Indium acetate; Zinc stearate; Zinc ethylxanthate; DDT; ODE; DMF	$CuInS_2/ZnS$	Ammonium hydroxide TEOS cyclohexane Igepal CO-520	25	[50]

Table 3. Summary and comparison different precursors and properties of synthesized polymer coated MQDs.

MNPs Precursor	**MNPs Composition**	**QDs Precursor**	**QDs Composition**	**MQD fabrication method**	**MQD Magnetism at (emu g^{-1})**	**Reference**
Iron (III) acetylacetonate phenyl ether OA	Fe_3O_4	CdO; zinc acetate; OA; ODE; TOP; Se powder; sulfur	Gradient CdSeS	Encapsulation of MNPs and QDs in mesoporous poly(styrene-co-EGDMA-co-MAA) beads	NA	[51]

oleylamine						
Iron(III) acetylacetonate OA; oleylamine	Fe_3O_4	As-received	CdSe	Encapsulation of MNPs and QDs in poly(PLA-TPGS)	NA	[52]
$FeCl_3.6H_2O$; Sodium oleate; Hexane; Ethanol; OA;ODE	Fe_3O_4	As-received	PbS	Encapsulation of MNPs and QDs in poly(lactic-co-glycolic-acid)	55	[53]
Polyethyleneimine $FeCl_2.4H_2O$ $FeCl_3.6H_2O$; NaOH	Fe_3O_4	TOPO; TOP; dimethylcadmium Se powder; diethyl zinc; $(TMS)_2S$	CdSe/ZnS	Covalent bond of MNPs-PEI with QDs MQDs yield 40-79%	50	[54]
$FeCl_2.4H_2O$ $FeCl_3.6H_2O$ Dextran Ammonium hydroxide	Fe_3O_4	Sodium diethyldithiocarbamate $AgNO_3$ $In(NO_3)_3$ $Zn(NO_3)_2$; oleylamine	$AgInS_2$/ZnS	Covalent bond of MNP with QDs		[55]
Poly(ethylene glycol) bis(carboxymethyl) ; ether; $FeCl_2.4H_2O$; $FeCl_3.6H_2O$; NaOH diethylene glycol	Fe_3O_4	Te powder $NaBH_4$ $CdCl_2.2.5H_2O$ MPA	CdTe	Covalent bond of MNP with QDs on CNT MQDs yield: 14%	50	[56]
$FeCl_2.4H_2O$; $FeCl_3.6H_2O$; Chitosan; Ammonium hydroxide; Acetic acid	Fe_3O_4	Zinc acetate; Manganese acetate tetrahydrate; $Na_2S.9H_2O$	ZnS:Mn	Encapsulation of MNPs and QDs in chitosan	10.5	[57]
$FeCl_2.4H_2O$; $FeCl_3.6H_2O$; Ammonium hydroxide; Sodium citrate	Fe_3O_4	$Cd(ClO_4)_2.6H_2O$; H_2Te TGA; NaOH	CdTe	LBL attachment of MNPs and QDs via electrostatic forces	65	[58]
$FeCl_2.4H_2O$; $FeCl_3.6H_2O$; Ammonium hydroxide; Lauric acid	Fe_3O_4	2-MPA; Na_2S; $AgNO_3$	Ag_2S	Covalent bond of MNP with QDs	7-9	[59]
As-received	Fe_3O_4	Te powder; $NaBH_4$; $CdCl_2$ Thiourea; GSH	CdTe	Covalent bond of MNP with QDs MQDs yield: 19.5%	NA	[60]

Iron (III); acetylacetonate; OA Oleylamine; Phenyl ether	Fe_3O_4	As-received	CdSe	Encapsulation of MNPs and QDs in poly(styrene-b-ethylene oxide)	NA	[61]
Iron(III) acetylacetonate; 1-Vinyl-2-pyrrolidone Ethanol; ether	Fe_3O_4	Dodecanethiol Indium(III) acetate; CuI zinc stearate	$CuInS_2$/ZnS	Covalent bond of MNP with QDs	NA	[62]
Iron(III); acetylacetonate; Manganese; acetylacetonate; 1,2-hexadecanediol benzyl ether; OA; oleylamine	$MnFe_2O_4$	Dodecanethiol; Indium(III) acetate; CuI; Zinc stearate TOP; ODE; Sulfur	$CuInS_2$/ZnS	Self-assembling of PEG-PLGA to form micellar MQDs; MQDs yield: 10%	NA	[63]
$FeCl_2.4H_2O$; $FeCl_3.6H_2O$: Ammonium hydroxide; PPA	Fe_3O_4	$ZnSO_4$ $MnCl_2$ Na_2S	Mn:ZnS	Covalent bond of MNP with QDs	40	[64]

3.2. Polymer coated MQDs

To prepare MQDs, polymer or organic materials can be used to encapsulate QDs and magnetic nanoparticles either by encapsulation of QDs and magnetic nanoparticles into polymer materials or polymerizing of monomers in the presence of nanocrystals or attachment of MNPs and QDs through covalent bond between MNPs and QDs. The different compositions of precursors and magnetic properties of polymer coated MQDs are summarized in Table 3.

Li et al. used poly(styrene-co-ethylene glycol dimethacrylate-co-methacrylic acid) beads (PSEMBs) to embed magnetic nanoparticles and QDs to fabricate multimodal hybrid nanoparticles by combining conventional swelling and high-temperature swelling methods [51]. In this process, highly crosslinked mesoporous PSEMBs beads were first synthesized using conventional swelling method and high temperature swelling was used to embed QDs in the MNPs-beads. This method was effective to prevent nanoparticles leakage problem in case of using organic solvent as the swelling agent and allow synthesis of MQDs with higher physical and chemical stability and rapid separation. The synthesized MNPs-QD-encoded polystyrene beads demonstrated immunoassay performance for detecting human IgG. The study revealed that carboxyl groups on fluorescent microsphere surface facilitated efficient attachment of biomolecule and therefore they can be further applied for rapid separation and multiplexed biomolecular assays [51]. Similarly, Tan et al. [52] encapsulated iron oxide nanoparticles and QDs inside a soluble polymer, poly(lactide)tocopherol polyethylene glycol succinate (PLA-TPGS) by a modified nanoprecipitation method for multimodal tumor imaging. They mixed QDs, iron oxide nanoparticles and PLA-TPGS in tetrahydrofuran (THF) then the solution was gradually added to aqueous phase containing tocopheryl polyethylene glycol (TPGS) as emulsifier with PLA providing mechanical strength and biodegradability, while TPGS enabled biocompatibility as well as provided multiple drug resistance inhibitor activity. This work demonstrated that co-encapsulation of QDs and iron oxide NPs in PLA-TPGS copolymers can be used for both of MRI and fluorescent imaging concurrently, which not only reduces the toxicity of the individual contrast agents and improve their biocompatibility, but also shields the contrast agents from detection by the human immune system. This allowed controlled delivery of imaging agents with passive targeting effects for the tumors.

Other type of MQDs used in MRI is reported by Ortgies el al. [53], where magnetic fluorescent hybrid nanostructures were synthesized using luminescent PbS QDs that emit signals in biological window (BW) II at wavelengths 1000-1350 nm. Both PbS QDs and iron oxide NPs were encapsulated in poly(lactic-co-glycolic-acid) (PLGA) polymer through a double emulsion technique, forming a water-in-oil-in-water emulsion, which after evaporation of the organic solvent and hardening of the capsules, led to precipitation of the hybrid nanostructures. This system was used for *in-vivo* MRI and deep tissue infrared

fluorescence imaging in living mice and magnetic heating for magnetic hyperthermia treatments. However, synthesized hybrid nanostructures required further improvement in order to achieve selective and targeted imaging as well as uniform bio-distribution of the nanohybrid system.

Notable other studies show the application of MQDs tethered with biomolecules with specific function have been reported for imaging cancer cells. For example, Lou et al. [54] synthesized multimodal magnetic-fluorescence hybrid nanoparticles for cell labelling. Here, Fe_3O_4 nanoparticles were capped with polyethyleneimine (PEI) and trioctylphosphine oxide (TOPO) capped CdSe/ZnS core/shell QDs were assembled on the surface of Fe_3O_4-PEI nanoparticles by displacement of TOPO with PEI because of amphiphilic and polycation characters of PEI. This was followed by functionalization of cell-penetrating transactivator of transcription (TAT) peptide (GRKKRRQRRRPQ) on the surface of hybrid nanoparticles for optical detection of cell separation with low toxicity to cells and rapid human lung cancer cells imaging. In another study, Koktysh et al. [55] synthesized magnetic-fluorescence hybrid imaging nanoprobe using covalent linking of the oxidized dextran shell of magnetic particles to the glutathione ligands of cadmium-free AgInS2/ZnS QDs (Figure 12). These water-soluble glutathione stabilized AgInS2/ZnS QDs presented a new class of cadmium-free multimodal imaging agents for simultaneous visible or NIR optical and MRI of mediastinal lymph nodes in mice [55].

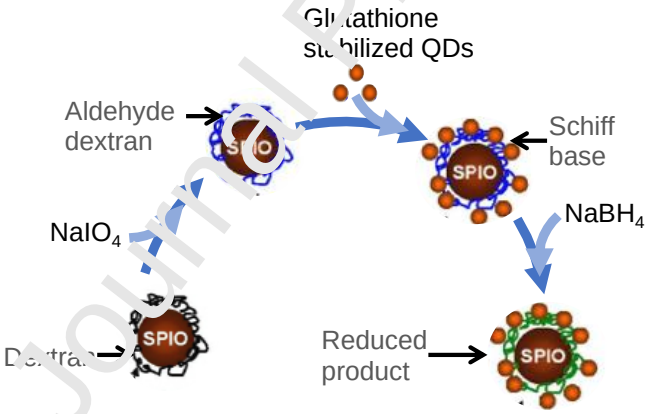

Figure 12. Schematic diagram illustrating the covalent linking of the oxidized dextran shell of SPIO nanoparticles with the glutathione ligands on QDs [55].

Cho et al. [65] conjugated amine functionalized QDs with emissions in the near-infrared range (800 nm) on carboxylate functionalized surface of a spherical polystyrene matrix encapsulated with superparamagnetic Fe_3O_4 NPs (MNs) (Figure 13). These magnetic-fluorescence hybrid nanospheres surfaces were loaded with Paclitaxel (PTX) drug using PLGA as the drug holder and drug release agent. This system was tested for cell viability of metastatic PC3mm2 prostate cancer cells by MTT assay in different concentration of the nanospheres. The results showed cell viability of PTX-PLGA-MQDs were

dose dependent while MNPs, MQDs and PLGA-MQDs were independent of nanoparticle concentrations. In the other experiment, PTX loaded polystyrene nanospheres were conjugated with antibodies for prostate specific membrane antigen (anti-PSMA) as targeting agent to obtain multifunctional nanospheres for fluorescent imaging, targeting, hyperthermia, and chemotherapy agent. Anti-PSMA on the surface of nanosphere successfully captured LNCaP prostate cancer cells. Moreover, these nanospheres were injected into tumor-bearing nude mice. Different fluorescent signals were obtained *ex-vivo* between tumor regions treated with the nanospheres and the nontargeted regions.

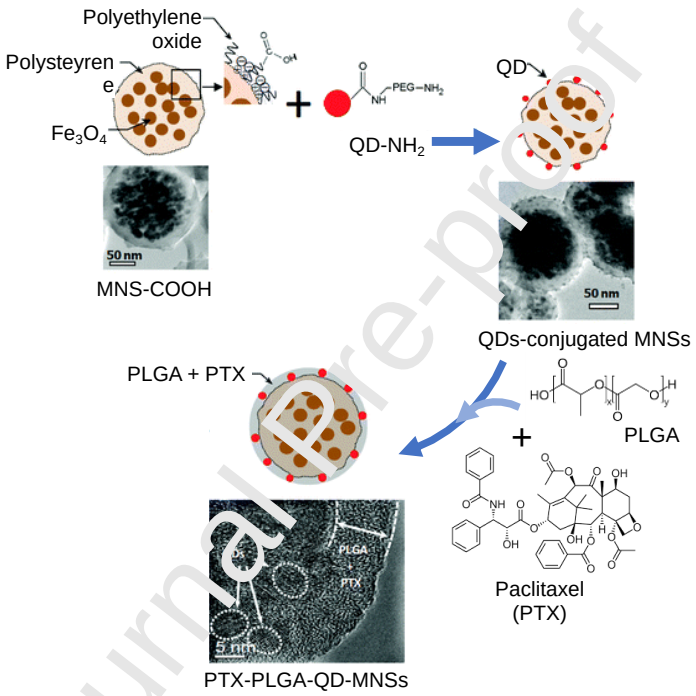

Figure 13. Attachment of amine-functionalized QDs to the surface of carboxylate-functionalized MNSs and loading of PTX on the surface of MQDs by formation a thin layer PLGA on the surface of MQDs [65].

Chen et al. [56] interfaced carbon nanotubes, superparamagnetic iron oxide nanoparticles and near-infrared fluorescent CdTe QDs by layer-by-layer (LBL) assembly in combination with covalent linking strategy. Here, multi-walled carbon nanotubes (MWCNTs) were functionalized with poly(allylamine hydrochloride) (PAH) and subsequently carboxyl terminated iron oxides were conjugated on the surface of MWCNTs. Again, PAH was used to functionalize the surface of MWCNT-iron oxide following conjugation with carboxyl terminated near infrared CdTe quantum dots in a layer-by-layer fashion. This system was used to detect human embryonic kidney (HEK) 293T cells and showed an enhanced MRI signal as contrast agent for detecting 293T cells in comparison with the pure superparamagnetic iron

oxide nanoparticles. This work also reported that the synthesized MWCNTs based magnetic Fe_3O_4-CdTe QDs system, magnetic Fe_3O_4 nanoparticles layer acted not only as a contrast agent for MRI, but also as a spacer between CdTe QDs and CNTs for prohibiting fluorescence quenching of QDs on the surface of the CNTs. In other study, Liu et al. [57] reported the preparation of chitosan (CS) coated magnetic-fluorescent nanoparticles (CS–Fe_3O_4@ZnS:Mn) using aqueous media under ambient pressure. Here, first Fe_3O_4 nanoparticles were coated with chitosan by co-precipitation of ferric and ferrous chloride salts in acetic acid aqueous solution of chitosan. Then, Zn^{2+} and Mn^{2+} ions were attached on the surface of chitosan due to electrostatic attraction between hydroxyl groups on the chitosan chains and positively charged metal ions. Subsequently, S^{2-} ions were added to the system in order to form ZnS:Mn quantum dots on the surface of chitosan (Figure 14). This method reported that the chitosan coating on the surface of Fe_3O_4 could effectively suppress the interaction between Fe_3O_4 and ZnS:Mn, as well as providing appropriate functional groups for the synthesis and modification of ZnS:Mn semiconductor nanocrystals for biomedical applications.

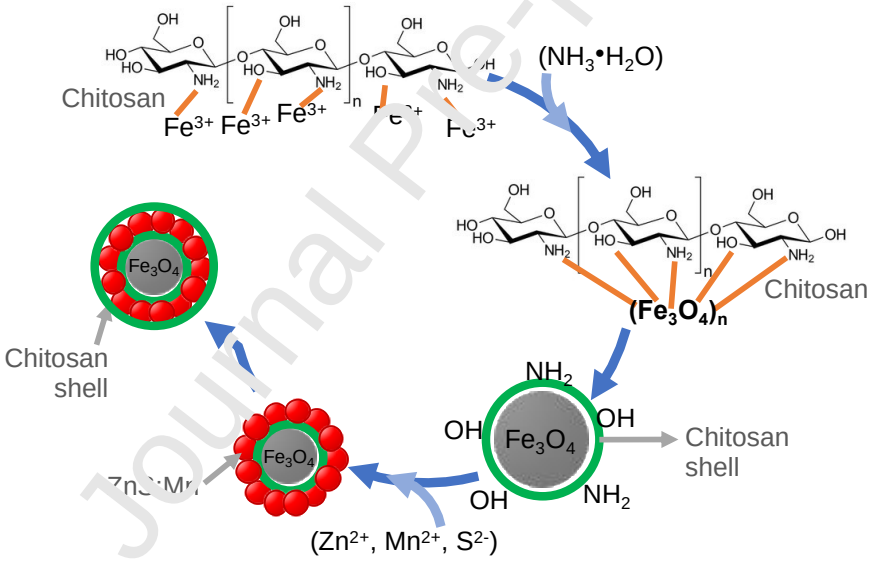

Figure 14. Schematic shows preparation of chitosan coated magnetic-fluorescent nanoparticles (CS–Fe3O4@ZnS:Mn) using aqueous media under ambient pressure [57].

Other studies showed chitosan shell matrix facilitated easy uptake of nanoparticles in cells, where iron oxide nanoparticles, CdS QDs and podophyllotoxin as an anti-cancer drug is encapsulated in chitosan nanospheres [66]. These hybrid nanospheres were tested *in-vitro* with human oral cancer (KB), rat glioma (C6) and human lung adenocarcinoma epithelial (A549) cells. Both fluorescence imaging and Perl's Prussian blue staining methods confirmed uptake of hybrid nanoparticles in oral cancer (KB) and glioma cells (C6) but not in lung adenocarcinoma cells (A549). A similar attempt was made by Ding et al. [67]

where chitosan based bimodal imaging and drug delivery system was fabricated which is composed of Fe_3O_4 MNPs, CdTe@ZnS QDs as a stable nanocomposite that exhibited excellent magnetic and fluorescence properties. Here, carboxymethyl chitosan (CMCS) was coated around Fe_3O_4 nanoparticles to minimize the possible fluorescence quenching triggered by magnetic cores. Then, CdTe/ZnS QDs were capped with glutathione (GSH) as a crosslinking agent to create chemical covalent conjunction between Fe_3O_4-CMCS, GSH-CdTe-ZnS and chitosan to enhance the stability of the nanocomposites for anti-cancer drug doxorubicin (DOX) release system (Figure 15). DOX release with nanocomposite drug delivery system was demonstrated to be pH dependent because of the solubility of chitosan at different pH-values and DOX was released maximum at pH = 5.3. The synthesized MQDs nanocomposite showed low cytotoxicity and the cell fluorescence labelling properties and time-dependent cellular uptake for bimodal imaging application.

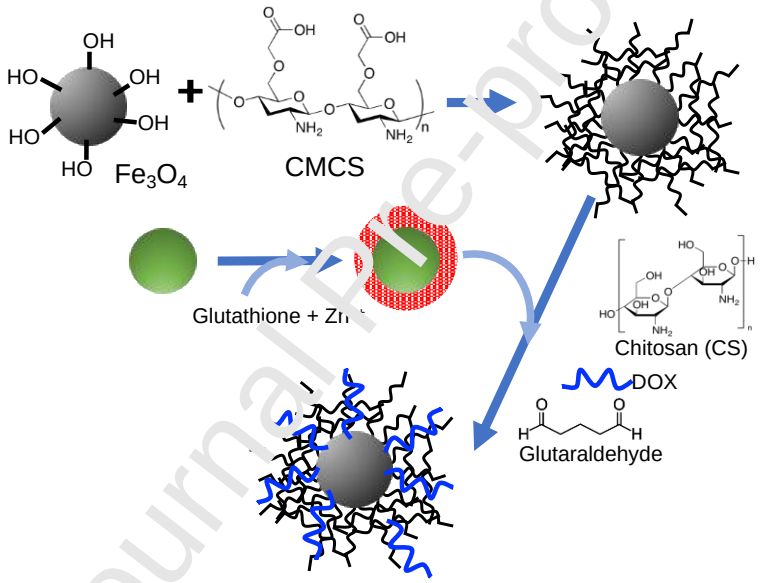

Figure 15. Schematic diagram of the fabrication steps for preparation of drug-loaded chitosan-based magnetic/fluorescent nanocomposites [67].

Ahmed et al. [58] used layer-by-layer self-assembly method to fabricate magnetic CdTe QDs for cancer cell imaging. In this method, citrate-capped negatively charged Fe_3O_4 nanoparticles were coated with cationic surfactant hexadecyltrimethyl ammonium bromide (CTAB) by electrostatic forces. Then, thioglycolic acid solution (TGA) capped CdTe QDs carrying negatively charged surface of QDs were electrostatically conjugated with CTAB. This system was used as fluorescence probe for LS174T human colon adenocarcinoma cancer cells after bioactivating QDs with humanized monoclonal antibody (hCC49) antibodies Fab region. This system was used for imaging colon carcinoma cells because of binding affinity of Fab region of hCC49 antibodies with sialylated sugar chain in TAG-72 region of

LS174T cancer cells. This nanosystem provided specificity to cancer cells along with magnetic and fluorescent features that is helpful in tracking, localizing and early diagnosis of cancers.

Hocaoglu et al. [59] synthesized near infrared magnetic fluorescence Ag_2S-Fe_3O_4 hybrid nanoparticles as cyto/hemocompatible system. This system was fabricated using 2-mercaptopropionic acid (2MPA) linkers with free carboxyl group on near infrared Ag_2S QDs in aqueous solution. Then magnetic Fe_3O_4 nanoparticles surface was coated with a monolayered lauric acid that enabled assembly of Ag_2S QDs by ligand exchange process between carboxyl group on the 2MPA and lauric acid. These nanohybrids exhibited interesting size dependent cytotoxicity behavior in HeLa and NIH/3T3 cell lines and almost no significant cytotoxicity in HeLa with 10 and 25 μg/mL Ag concentration but the same concentration was most toxic to mouse fibroblast cells (NIH/3T3) cells.

A different approach is reported that utilized DNA oligomers or aptamers for capturing and ultrasensitive detection of tumor cells. For example, DNA templated magnetic nanoparticle-QD polymers were synthesized for ultrasensitive capture and detection of circulating tumor cells by Li et al. [60]. Here, CdTe and CdTe-CdS QDs were capped with chimeric DNA1 (C1): 5′-(G*) 10(A) 6CGTCCGTGCTCAC-3′ templates or with chimeric DNA2 (C2): 5′-TCCTAGACGCGTA (A) 6(G*) 10(A) 6GTCGGAC GTGCAG-3′ templates. Fe_3O_4 nanoparticles capped with NH_2-modified DNA3 (C3): 5′-TACGCGTCTAGGATCAAAAAAAAAAA-NH2 3′ templates. Then, C1 DNA-CdTe/CdS QDs were mixed with C3 DNA-Fe_3O_4 nanoparticles and aptamer DNA to synthesize a complex of magnetic nanoparticles (MQAP). These MQAPs used for magnetic isolation of rare cancer cells with high capture efficiency and capture purities that are favorable for practical use. These MQAPs showed high magnetic response, selectivity, and photoluminescence intensity for simultaneous isolation and identification of circulating tumor cell under complex conditions.

Cheng et al. [68] synthesized QD/Fe_3O_4/Taxol(paclitaxel)-loaded PLGA NPs nanosystems for combination of chemotherapeutic and photothermal therapy in mammalian cells and in vivo in an animal model. QD/Fe_3O_4/Taxol-loaded PLGA system was synthesized by conjugating the stabilizer-free Taxol (paclitaxel)-loaded PLGA NPs with amine-terminal Fe_3O_4 NPs (~6 nm) and QDs (~12 nm). Followed by electrostatic attachment of negatively charges poly(styrenesulfonate) (PSS)-coated Au nanorods (aspect ratio of 3.9) on the PLGA-Taxol-Fe_3O_4-QDs because of positively charged functionalized amine groups from QDs and Fe_3O_4 nanoparticles surface. Then positively charged anti-Her2 antibodies was absorbed on the surface of negatively charged PSS-Au nanorods electrostatically to achieve selective HeLa cancer cells targeting for *in-vitro* and *in-vivo* evaluation of therapeutic performance. Photo-thermal destruction was achieved by near infrared irradiation and conversion of light to heat by Au nanorods because of melting and degradation of PLGA following Taxol release, while Fe_3O_4 nanoparticles and QDs was used for MRI and confocal imaging of cancer cells, respectively. This designed system was more effective

cancer cell treatment in combination of photo-thermal destruction and chemotherapy in comparison to photo-thermal destruction or chemotherapy alone.

Yin et al. [69] reported on a unique microfluidic synthesis of bifunctional magnetic-fluorescent responsive Janus supraballs. They synthesized an isotopic structure composed of poly(MMA-co-HEMA)/CdS QD–polymer hybrids hemisphere and magnetic Fe_3O_4 nanoparticles with poly(MMA-co-HEMA)/Cd $(AA)_2$ ionomer hemisphere. The microfluidic device consists of two needles in a microchannel that were used to simultaneously force flow two different oil solutions (QD–polymer hybrids-dichloromethane and ionomers containing Fe_3O_4-dichloromethane) (Figure 16(I-a). An aqueous solution of polyvinyl alcohol (PVA) was used as the continuous phase (water phase) externally. The two oil streams breaks into a pair of drops that immediately combine into a larger droplet at the exit tip in the outer water phase. The water contains PVA that served as a surfactant to prevent the oil micro particles from spreading on the surface of the collecting container. An external magnetic field in different directions is able to rotate these magneto-responsive Janus particles with distinct hemispherical regions of fluorescence and magnetic properties (Figure 16(IIa-j) [69].

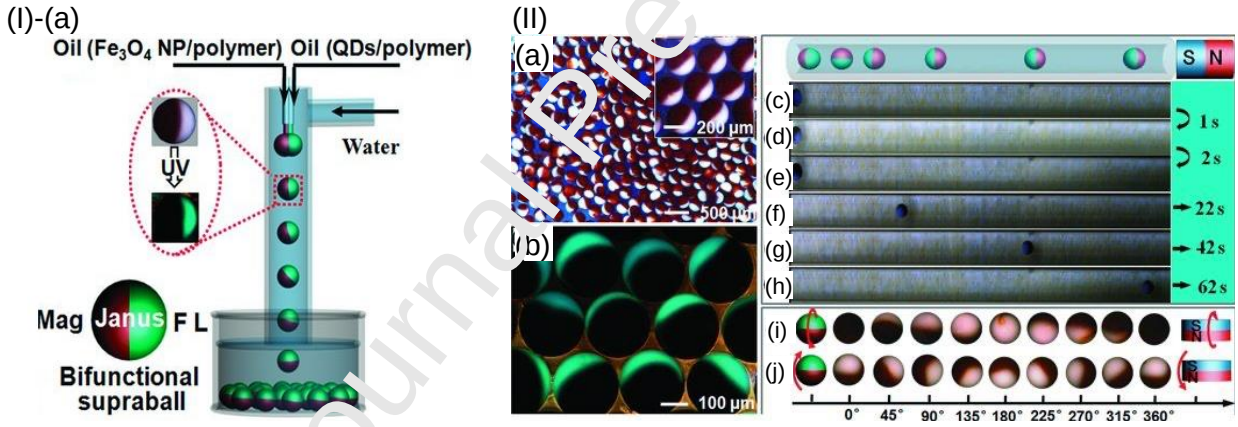

Figure 16. (I) (a) Schematic representation of microfluidic systems consists of two needle microchannel and was used to force to flow two different oil solutions of QD–polymer hybrids-dichloromethane and ionomers containing Fe_3O_4-dichloromethane, simultaneously for the synthesis of monodisperse Janus supraballs. (II) (a) Optical and (b) fluorescence microscopy images for Janus supraballs. (c–h) Movement of Janus supraballs in a capillary tube toward an additional magnet at different intervals. (i-j) Schematic illustration and optical images showing rotational motion of Janus supraballs under an external magnetic field induced by a rotating magnet [69].

Ruan et al. [61] reported "nano-conveyer-belt" platform technology composed of polymeric micelle nanocontainers (~35 nm) encapsulating separate QDs and iron oxide nanoparticles (HMQDs) for simultaneous manipulation and optical tracking of multiple nanostructures in a selected direction.

Nanocontainers encapsulated HMQDs were synthesized by interfacial instability method in which first water-soluble micelles with hydrophobic cores were prepared by dissolving amphiphilic block copolymers in chloroform (organic, water-immiscible solvent), and were later dispersed in aqueous solution. QDs and superparamagnetic Fe_3O_4 NPs with hydrophobic surfaces were incorporated into the hydrophobic cores by addition to the initial, organic phase. The numbers of QDs and superparamagnetic Fe_3O_4 NPs in each micelle were controlled by the molecular structure of the polymer employed and the quantities of polymer, QDs and Fe_3O_4 MNPs. Further, they fabricated magnetic nano-conveyers followed by sputtering of Fe-Co alloy and patterned as microdisks or magnetic nanowires on a silicon wafer. The HMQDs were introduced on the Fe-Co sputtered patterns and the path of magnetic-fluorescence hybrid nanoparticles was manipulated by applying and adjusting the current in the electric coil. This study demonstrated the unique fluorescent properties of constituent QDs that permitted imaging and tracking of HMQD-filled nanocontainers which potentially be used for therapeutic and micro/nanofluids, bio-labeling and imaging applications. Fan et al. [70] synthesized CdSe-ZnS QDs capped Fe_3O_4 magnetic nanorings for multiphoton fluorescence and MR imaging. First, they synthesized α-Fe_2O_3 nanoring by hydrothermal treatment of $FeCl_3$. Then α-Fe_2O_3 nanoring was annealed in the mixture of H_2 and Ar gases to reduce to Fe_3O_4 nanorings (NR). These nanorings were dispersed in water at pH 3, then citric acid was added to make these nanorings water soluble (Figure 17-a). Core-shell CdSe-ZnS QDs capped with polyethyleneimine (PEI) were synthesized by mixing PEI in absolute ethanol then added the QDs in chloroform solution. This mixture is then ultrasonicated and stirred to replace trioctylphosphine oxide (TOPO) capped QDs with PEI. In order to synthesize QDs capped magnetite nanorings, positively charged PEI capped QDs were added to aqueous solution of negatively charged citric acid capped Fe_3O_4 nanorings to obtain water dispersible QDs capped ferrimagnetic vortex-state iron oxide nanorings (QD-FVIOs). The magnetic resonance of these MQDs was done *in vitro* by dispersing MQDs in 2% agarose solution. The multiphoton fluorescence imaging and cell uptake of QD-FVIOs using MGH bladder cancer cells demonstrated that these QD-FVIOs could penetrate endosomes and released into the cytoplasm (Figure 17b(i-ii)). Moreover, normal human lung fibroblast cells (NHLF), MGH bladder cancer cells, and SK-BR3 breast cancer cells were used for *in vitro* cytotoxicity. However, PEI polymer limits the practical application of synthesized QD-FVIOs because of cytotoxicity for MGS cancer cells and further tailoring in surface chemistry of MQDs are required such as use of biocompatible polymer (PEG) for practical biomedical applications.

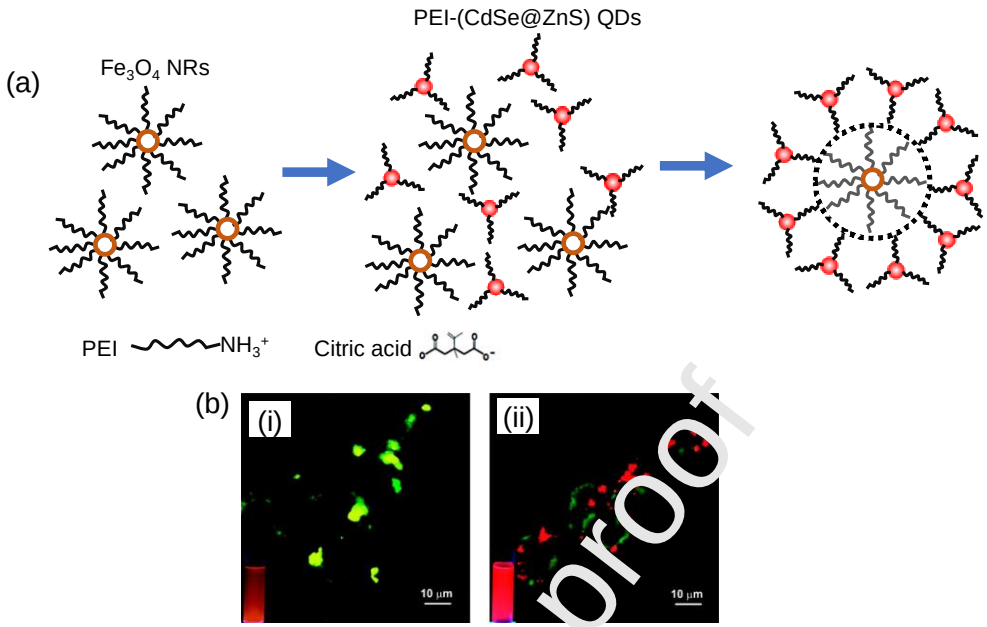

Figure 17. (a) Schematic illustration for the synthesis of water-dispersible QDs capped ferrimagnetic vortex-state iron oxide (QD-FVIO) nanorings (NRs). The branched PEI is drawn as line for simplification. (b) Two-photon fluorescence image (756 nm excitation) of the stained MGH bladder cancer cells with (i) yellow- and (ii) red-colored internalized QD-FVIOs [70].

In another study, $CuInS_2$-ZnS QDs were coated with the amphibious Fe_3O_4 nanoparticles by a simple approach [62]. First, hydrophobic $CuInS_2$-ZnS QDs were prepared through a self-assembling process induced by introducing indium (III) acetate and copper (I) iodide in 1-dodecanethiol under nitrogen flow at 200 ºC. ZnS shell was formed by adding zinc stearate to the $CuInS_2$ solution under nitrogen at 230 º C and the core-shell QDs were precipitated and washed with ethanol and finally dissolved in cyclohexane (Figure 18). It was reported that the size of $CuInS_2$-ZnS QDs can be tuned by manipulating the nucleation and the growth kinetics through the addition rate of ethanol. Then, the amphibious Fe_3O_4 nanoparticles stabilized with poly(4-vinylpyrollidone) (PVP) was synthesized by dissolving iron (III) acetylacetonate in 1-vinyl-2-pyrrolidone (NVP) at 200 ºC under the nitrogen (Figure 18). The resulted nanoparticles were dissolved and precipitated by ethanol and ether several times to obtain amphibious Fe_3O_4 nanoparticles in ethanol. In order to coat hydrophobic QDs with amphibious Fe_3O_4, the magnetic nanoparticles were added to QDs solution dropwise then centrifuged and dispersed in DI water (Figure 18).

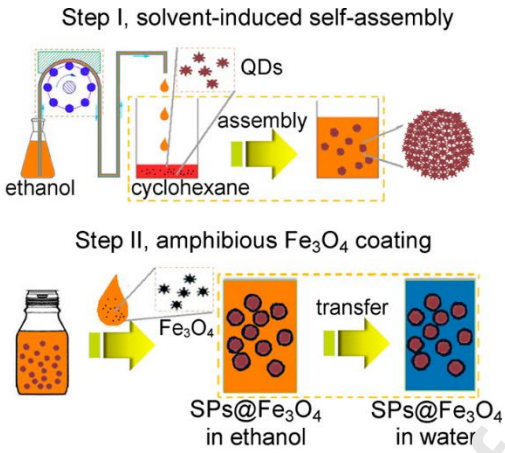

Figure 18. step I: preparation of hydrophobic $CuInS_2$@ZnS QDs; step II: amphibious coating of Fe_3O_4 around QDs followed dispersion in the water [62].

Shibu et al. [71] synthesized multimodal and multifunctional photouncaging MQDs using photouncaging ligand. At first, they prepared biotin-functionalized Fe_3O_4 nanoparticles using the biotin moieties conjugated to streptavidin-functionalized Fe_3O_4 nanoparticles. Then streptavidin-functionalized CdSe-ZnS QDs was conjugated to biotin-functionalized Fe_3O_4 nanoparticles by adding biotin-functionalized Fe_3O_4 to a QD solution and incubated at 37 °C for 2 h to obtain photouncaging bimodal nanoparticles as the MQD. Bimodal imaging and cytotoxic effects of as-synthesized MQDs were carried out with biotinylated allatostatin I (peptide hormone) using 3-sulfo-*N*-hydroxysuccinimide ester of biotin and subsequently conjugated to streptavidin moieties of MQDs. *In vivo* MRI and fluorescence images of B6 mice either subcutaneously or intravenously injected with the photouncaging nanoparticles showed magnetic and fluorescence contrast enhancements under the skin or in the liver. These nanoparticles tend to disappear within 48 h according to MRI and fluorescence images taken from the liver, urinary bladder and urine samples at different time intervals.

Demillo et al. [63] fabricated MQDs using $MnFe_2O_4$ magnetic nanoparticles (MNPs), $CuInS_2$/ZnS QDs and poly(ethylene glycol)-*b*-poly(lactide-co-glycolide) (PEG-PLGA) in a tetrahydrofuran (THF)/water solvent system. Here, $MnFe_2O_4$ MNPs were synthesized through a thermal decomposition method. $CuInS_2$/ZnS QDs were synthesized using a revised thermal decomposition method. To fabricate MQDs, $MnFe_2O_4$ MNPs, $CuInS_2$/ZnS QDs were co-encapsulated within PEG-PLGA micelles using quick solvent THF displacement solution and cooled using cold water and sonicated for 1 min (Figure 19). After sonication, THF in the medium was evaporated using room temperature rotary evaporation method. The empty micelles or single-nanoparticle based micelles were separated by centrifugation and obtained MQDs dispersion. The fabrication process is schematically shown in Figure 19. It was demonstrated that

MQDs nanocomposite possess high (Mn + Fe) recovery rates, which further makes the fabrication cost lower without compromising optical properties and magnetic relaxivity, which can be tuned by adopting different MNP:QD mass ratios during fabrication. The MQDs prepared with this method exhibited a minimal cytotoxicity and excellent capability of bioconjugation for variety of biological applications.

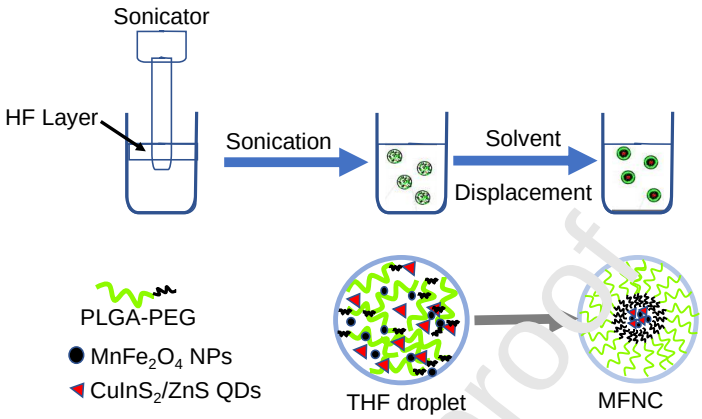

Figure 19. MQD fabrication process using PEG-PLGA, $MnFe_2O_4$ MNPs and $CuInS_2$/ZnS QDs in THF/water. Through sonication and quick solvent displacement, multiple nanoparticles of each type are co-encapsulated within the hydrophobic core of PEG-PLGA micelle [63].

Martynenko et al. [72] synthesized MQDs microbeads for bacteria detection and these microbeads were composed of fluorescent Cd-free Ag–In–S ternary quantum dots (t-QDs) with fluorescence lifetimes (LTs) of several hundred nanoseconds and coated with superparamagnetic Fe_3O_4 nanoparticles with mesoporous $CaCO_3$ microbeads. $CaCO_3$ microbeads were first synthesized by chemical reduction of $CaCl_2{\cdot}2H_2O$ using micelles that were made from polyvinylpyrrolidone (PVP) and sodium dodecyl sulfate (SDS) as templates. In a separate reaction, poly(sodium 4-styrenesulfonate) (PSS) capped Fe_3O_4 MNPs were synthesized by chemical precipitation of $FeCl_3{\cdot}6H_2O$ and $FeCl_2{\cdot}4H_2O$ in the presence of PSS and Na_2CO_3. Subsequently, the porous $CaCO_3$ beads were incubated with PSS-capped magnetic Fe_3O_4 NPs, which provided brownish to Fe_3O_4@$CaCO_3$ particles with negative surface charges (Figure 20). The core/shell AgInS2/ZnS QDs capped with hydrophilic ligand mercaptopropionic acid were used as optical codes and these were synthesized using a microwave-assisted aqueous route. In the next step, negatively charged MPA coated AgInS/ZnS QDs were electrostatically deposited on positive charged Fe_3O_4@$CaCO_3$ beads by the alternating deposition of poly(allylaminehydrochloride) (PAH) and PSS (Figure 20). The fabricated $CaCO_3$@Fe_3O_4@AIS/ZnS microbeads in this study were used to demonstrate immuno-magnetic capturing of *L. pneumophila* cells.

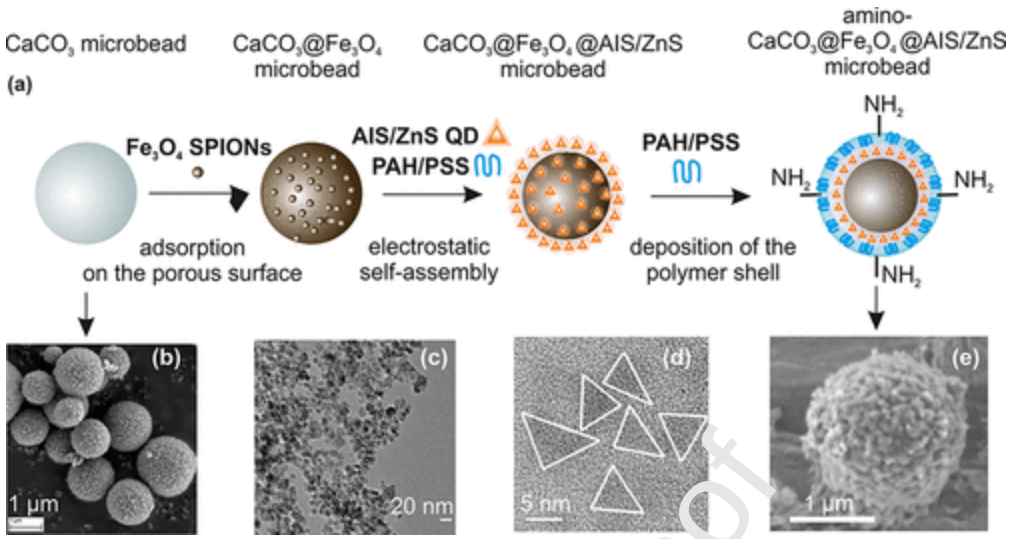

Figure 20. (a) Schematic illustration of synthesis procedure steps of aminated magneto-AIS/ZnS QDs-$CaCO_3$ microbeads. SEM and TEM images of (b) $CaCO_3$ spherical microparticles, (c) PSS-capped magnetic Fe_3O_4 NPs, (d) AIS/ZnS QDs capped with MPA, and (e) $CaCO_3$@Fe_3O_4@AIS/ZnS microbeads with amino surface groups [72].

MQDs of different composition have also found to be applicable to capture and detect ultra-trace amount so chemicals in water. For example, Zhu et al. [64] synthesized MQDs composed of Fe_3O_4 MNPs and Mn-doped ZnS QD nanocomposites (MNPs/QD NCs) for room-temperature phosphorescence sensing and magnetic separation of captured ultratrace 2, 4, 6-trinitrotoluene in water. This study utilized coprecipitating method to prepare bare Mn-doped ZnS QDs followed by grafting mercapto groups of mercaptoethanylamine due to the excess of metal ions with respect to sulfide ions at the surface of the QDs. Phosphonopropionic acid (PPA) capped Fe_3O_4 MNPs were synthesized by coprecipitation method separately. The as-synthesized MNPs were functionalized with EDC and NHS followed by the addition of MEA capped Mn doped ZnS QDs to solution and obtained unique superparamagnetism, and decoration of QDs with grafted MEA endow the MNPs/QD NCs with high surface-to-volume ratio. This study showed the ability of magnetic and chemosensory property of synthesized MNPs/QD NCs by magnetically concentrating TNT in water.

In a recent study from our laboratory, we demonstrated a unique nanoarchitecture of MQDs synthesized using CdSe/Cds/ZnS core-shell-shell QD nanocrystals and MNPs by systematic sequential chemical conjugation process that gave rise to specific orientation in which central QD nanocrystals were decorated on its surface with MNPs [73]. This sequential arrangement of nanostructures was accomplished by following steps, where (a) gradient synthesis of CdSe/CdS/ZnS QD nanocrystals

containing core CdSe with gradient shells of CdS followed by ZnS. (b) CdSe/CdS/ZnS QDs were subjected to surface activation by ligand exchange reaction process with CS_2 and glycine that formed a polymeric coating with free carboxyl functionality on QDs' surface and provided hydrophilicity. These hydrophilic QDs were then chemically conjugated with L-aspartate capped magnetic Fe_3O_4 nanoparticles that were previously synthesized by hydrothermal process. As a result, CdSe/CdS/ZnS QDs were decorated with MNPs yielding ~100-200 nm sized MQDs that proved to be excellent nanoprobes with multifunctionality for PoC applications (Figure 21).

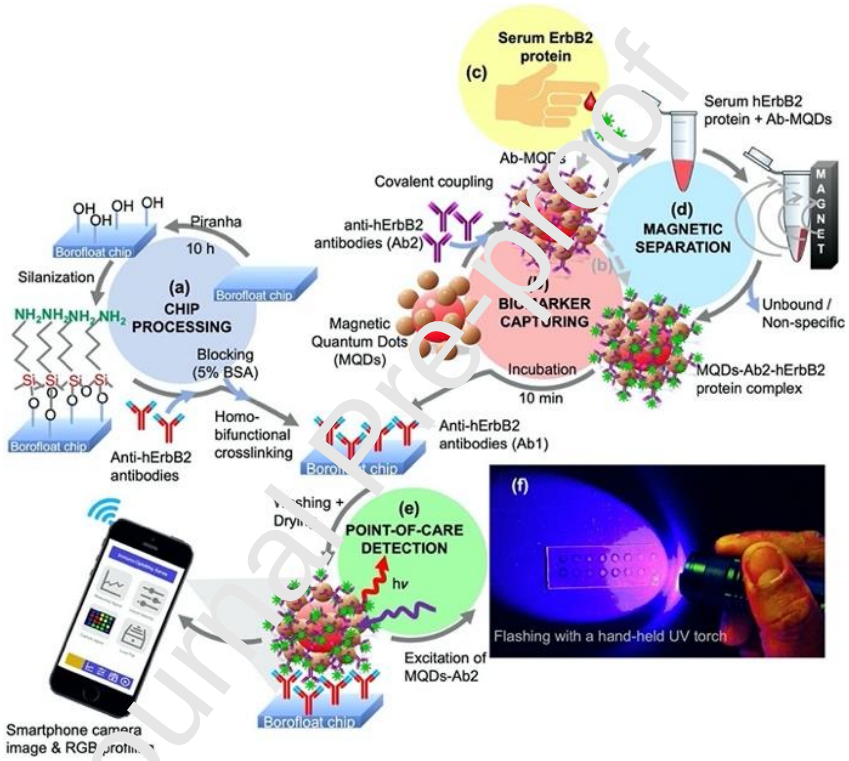

Figure 21. Schematic illustration of point-of-care (PoC) immuno-optomagnetic assay developed for detecting disease biomarker protein from a real serum using CdSe/CdS/ZnS@Fe_3O_4 magnetic quantum dots (MQDs), where QDs were shielded by surrounding magnetic Fe_3O_4 nanoparticles. These MQDs served as excellent multimodal nanostructures with optical, magnetic and biological functionalities in PoC detection. The scheme shows series of steps (a-f) involved in detection of diagnostic signal by naked eye [73].

Table 3. Summary and comparison different precursors and properties of synthesized polymer coated MQDs.

MNPs Precursor	***MNPs Composition***	***QDs Precursor***	***QDs Composition***	***MQD fabrication method***	***MQD Magnetism at (emu g^{-1})***	***Reference***
Iron (III) acetylacetonate phenyl ether OA oleylamine	Fe_3O_4	CdO; zinc acetate; OA; ODE; TOP; Se powder; sulfur	Gradient CdSeS	Encapsulation of MNPs and QDs in mesoporous poly(styrene-co-EGDMA-co-MAA) beads	NA	[51]
Iron(III) acetylacetonate OA; oleylamine	Fe_3O_4	As-received	CdSe	Encapsulation of MNPs and QDs in poly(PLA-TPGS)	NA	[52]
$FeCl_3.6H_2O$; Sodium oleate; Hexane; Ethanol; OA;ODE	Fe_3O_4	As-received	PbS	Encapsulation of MNPs and QDs in poly(lactic-co-glycolic-acid)	55	[53]
Polyethyleneimine $FeCl_2.4H_2O$ $FeCl_3.6H_2O$; NaOH	Fe_3O_4	TOPO; TOP; dimethylcadmium Se powder; diethyl zinc; $(TMS)_2S$	CdSe/ZnS	Covalent bond of MNPs-PEI with QDs MQDs yield: 40-79%	50	[54]
$FeCl_2.4H_2O$ $FeCl_3.6H_2O$ Dextran Ammonium hydroxide	Fe_3O_4	Sodium diethyldithiocarbamate $AgNO_3$ $In(NO_3)_3$ $Zn(NO_3)_2$; oleylamine	$AgInS_2$/ZnS	Covalent bond of MNP with QDs		[55]
Poly(ethylene glycol) bis(carboxymethyl) ether; $FeCl_2.4H_2O$; $FeCl_3.6H_2O$; NaOH diethylene glycol	Fe_3O_4	Te powder $NaBH_4$ $CdCl_2.2.5H_2O$ MPA	CdTe	Covalent bond of MNP with QDs on CNT MQDs yield: 14%	50	[56]
$FeCl_2.4H_2O$; $FeCl_3.6H_2O$; Chitosan; Ammonium hydroxide; Acetic acid	Fe_3O_4	Zinc acetate; Manganese acetate tetrahydrate; $Na_2S.9H_2O$	ZnS:Mn	Encapsulation of MNPs and QDs in chitosan	10.5	[57]
$FeCl_2.4H_2O$; $FeCl_3.6H_2O$; Ammonium hydroxide; Sodium citrate	Fe_3O_4	$Cd(ClO_4)_2.6H_2O$; H_2Te TGA; NaOH	CdTe	LBL attachment of MNPs and QDs via electrostatic forces	65	[58]

$FeCl_2.4H_2O$; $FeCl_3.6H_2O$; Ammonium hydroxide; Lauric acid	Fe_3O_4	2-MPA; Na_2S; $AgNO_3$	Ag_2S	Covalent bond of MNP with QDs	7-9	[59]
As-received	Fe_3O_4	Te powder; $NaBH_4$; $CdCl_2$ Thiourea; GSH	CdTe	Covalent bond of MNP with QDs MQDs yield: 19.5%	NA	[60]
Iron (III); acetylacetonate; OA Oleylamine; Phenyl ether	Fe_3O_4	As-received	CdSe	Encapsulation of MNPs and QDs in poly(styrene-b-ethylene oxide)	NA	[61]
Iron(III) acetylacetonate; 1-Vinyl-2-pyrrolidone Ethanol; ether	Fe_3O_4	Dodecanethiol Indium(III) acetate; CuI zinc stearate	$CuInS_2$/ZnS	Covalent bond of MNP with QDs	NA	[62]
Iron(III); acetylacetonate; Manganese; acetylacetonate; 1,2-hexadecanediol benzyl ether; OA; oleylamine	$MnFe_2O_4$	Dodecanethiol; Indium(III) acetate; CuI; Zinc stearate TOP; ODE; Sulfur	$CuInS_2$/ZnS	Self-assembling of PEG-PLGA to form micellar MQDs; MQDs yield: 10%	NA	[63]
$FeCl_2.4H_2O$; $FeCl_3.6H_2O$: Ammonium hydroxide; PPA	Fe_3O_4	$ZnSO_4$ $MnCl_2$ Na_2S	Mn:ZnS	Covalent bond of MNP with QDs	40	[64]

4. Synthesis of MQDs by doping of QDs with iron ions

Doping of QDs with paramagnetic transition metal ions is another method to synthesize MQDs. The most important challenge in doping method is introducing a few of atoms inside the crystal lattice of a few hundred atoms of metal NPs without the clustering of dopant ions on the surface or inside the QDs [33]. Saha et al. [74] synthesized Fe_3O_4 core based CdS MQD by diffusion of the Fe_3O_4 out of the CdS matrix. This study utilized controlled engineering strategy by controlling annealing temperature as well as the reaction coefficient of precursors. Therefore, diffusion of the magnetic ions could occur slower than the growth of the semiconductor lattice leading in order to obtain controlled diffusion of the magnetic ions. The successive ionic layer adsorption and reaction (SILAR) technique was used to grow with controlled diffusion of Fe ions inside the thick matrix of CdS nanostructure. Arresting of the diffusion before the complete expulsion of the dopant ions lead to formation of Fe-doped CdS QDs with excellent control over their size distribution, uniformity of dopant ions and percentage of doping (Figure 22a-b). TEM examination showed that sizes obtained as a function of growth of CdS nanocrystals around the core Fe_3O_4 nanocrystals ranged from 4.5 nm (Figure 22a) to 8.5 nm, 12.6 nm and 15.4 nm (Figure 22b(i-iv)) respectively. The particles are spherical and have fairly uniform size distribution signifying a uniform growth of nanocrystals and iron percentage with 5, 10 and 14 cycles of Cd and S additions, respectively.

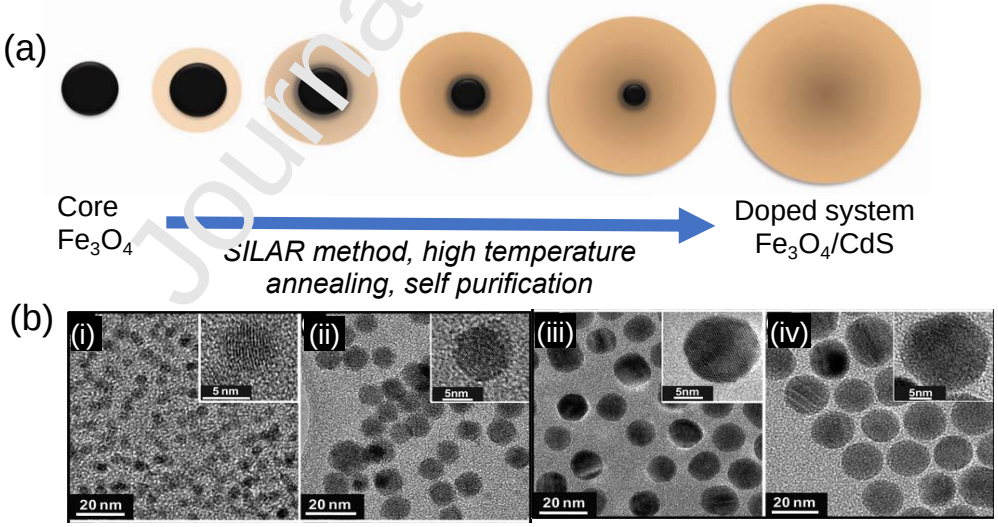

Figure 22. (a) Schematic showing synthesis procedure of Fe_3O_4 core based diffusion of dopants into the CdS matrix to obtain Fe-doped CdS QDs. (b) TEM images showing (i) 4.5 nm Fe_3O_4 core, (ii) Fe-5CdS, (iii) Fe-10 CdS, (iv) Fe-14 CdS, Results show that iron doping with 5, 10 and 14 cycles of Cd and S additions, respectively. [74].

5. Miscellaneous methods for MQDs synthesis

Liu et al. synthesized superparamagnetic nitrogen- doped carbon- iron oxide hybrid QDs (C- Fe_3O_4 QDs) for *in vivo* triple modal bioimaging by fluorescence, magnetic resonance and computer tomography (FL/MR/CT) [75]. This work used a green and facile one- pot hydrothermal method by using poly(γ-glutamic acid) as a precursor and stabilizer agent. At first, ferrous chloride tetrahydrate ($FeCl_2.4H_2O$), ferric chloride hexahydrate ($FeCl_3.6H_2O$) were dissolved in deionized water following addition of poly-γ-glutamic acid (γ-PGA) to the solution. Then nitrogen was bubbled inside the solution and solution was stirred for 3 h. Afterward the solution temperature was raised to 60 ºC and the pH solution was adjusted to 10 using ammonium hydroxide solution and the solution was kept at 60 ºC for another 5 h. Finally, the mixture was transferred to a Teflon-lined autoclave and maintained at 180 ºC for 8 h. The autoclave was cooled naturally to the room temperature and the obtained solution was dialyzed against deionized water for one day followed by freeze-drying to collect formed nitrogen doped carbon MQDs. Theses MQDs showed excellent water dispensability, quantum yield, strong magnetic properties and good biocompatibility. Cell cytotoxicity assessment using HeLa cells in different MQDs concentration exhibited very good cell viability up to 500 μg/mL of MQDs. The *in-vivo* fluorescence, magnetic resonance, and computed tomography bioimaging studies demonstrated that these MQDs can be used as a potential contrast agent for triple-modal FL/MR/CT imaging of tumors.

Li et al. [76] synthesized satellite structure of microsphere silicon oxide microspheres (SiMS) assembled with Fe_3O_4 NPs and CdTe QDs by LBL assembly and thiol covalent coupling, respectively. At first, SiO_2 microspheres modified by thiol group (SiMS) were prepared by treating microsphere with (3-mercaptopropyl) trimethoxysilane (MPS) dropwise to functionalize the surface of silica with thiol groups. The purified thiol functionalized silica microspheres solution was mixed dropwise with Fe_3O_4 MNPs in a span of 24 h to form SiMS-MNPs. The surface of SiMs-MNPs was thiol functionalized by mixing 1, 6-dimercaptohexane (DMH) solution in anhydrous toluene with SiMS-MNPs solution followed by layer-by-layer assembly of MNPs on the surface of SiMS-MNPs to add more MNPs. A mixture of TEOS and MPS was added dropwise into the solution in 3 h span to form a silica layer with thiol groups on the surface as SiMS-MNPs-SiO_2 (Figure 23). In a separate reaction, CdTe QDs were synthesized by adding tellurium powder in DI water and $NaBH_4$ in the ice bath under vacuum in 2 h to form NaHTe. On the other hand, a solution of cadmium chloride and thioglycolic acid (TA) was prepared at 100 ºC and the pH was adjusted to 10, then NaHTe solution was added to this solution and the reaction was continued for 20 h. TA stabilized CdTe QDs were precipitated in acetone, purified and re-dispersed in DI water. These TA stabilized QDs were added dropwise to the aqueous solution of SiMS-MNPs-SiO_2 which functionalized

with MPS and the pH was adjusted to 11, then the reaction was continued for 4 h to generate SiMS-MNPs-SiO_2-CdTe composite. Figure 23 shows schematic illustration of the synthesis of core-shell composite.

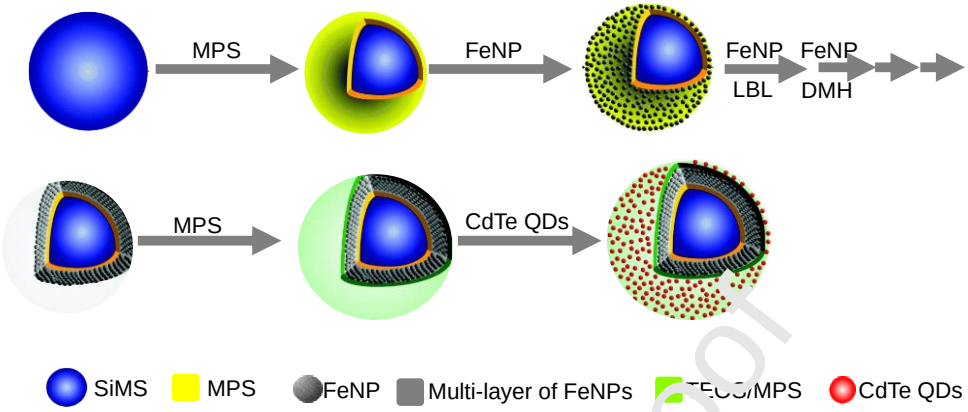

Figure 23. Preparation steps of the core–shell–satellite structured of MQDs [76].

6. Conclusions and perspectives

MQDs synthesized by chemical combination of QDs and MNPs provide unique multimodal functionality because of their excellent combination of optical and magnetic properties that is most desirable feature applicable in many biomedical and biological applications, such as bio-labeling, MR imaging, hyperthermia treatments, chemotherapy, disease diagnostics, drug delivery, sorting and separation processes. In this review, we presented recent strategies that have been employed for chemical synthesis and integration of Fe_3O_4 MNPs and QDs. Most common approaches are those of first, QDs synthesis utilizing Cd or Pb elemental sources in organic solution via high temperature injection. However, QDs with Cd or Pb are not suitable for bio-medical applications because of their heavy metal toxicity. A few studies have focused on synthesis of Cd/Pb-free QDs and these were made of non-toxic InP, $CuInS_2$, Ag_2Se or AgS, however they suffer from low quantum yield and broad emission spectra. These features can be improved through incorporating Se and In elements during their synthesis, but doping of these elements further limits their biocompatibility. Direct QDs synthesis in water or other hydrophilic solvents is a promising approach to synthesize core-shell QDs and MNPs doped nanomaterial to obtain MQDs. Carbon dots are other nontoxic materials that has been synthesized using a green chemistry method which is inexpensive and scalable, but requires more investigation in order to improve their optical properties and stability. Fluorescence emission of carbon dots depends on their defects, therefore, manipulating the surface of carbon dots to create specific density, defects in specific spots along with their controlled size and shape requires systematic investigation to improve optical properties.

Synthesis of MNPs and alloying iron with other elements to obtain stronger magnetic moment, as well as synthesis of QDs with higher QY will allow fabricating MQDs most suitable for *in vivo* applications. Recent attempts to synthesizing MQDs with unique nanoarchitecture and orientations could play a vital role in their biological and/or biomedical applications with minimum or no toxicity. For instance, CdSe/CdS/ZnS QDs remain buried while being protected by surrounding MNPs. Such type of CdSe/CdS/ZnS@MNPs are not only highly stable, bright and magnetic, but also prevent from release/dissociation of QDs from MQDs due to a strong protective shield formed by the MNPs decorated around core QDs. Such MQDs carry multi-functionality of magnetic, optical and biological functionality post-bioactivation. Biocompatibility and performance of MQDs depends on additional factors, such as their shape, surface charge, size, ligands and surface coating materials. Additionally, integrating such MQDs and handling small volume of samples with the aid of microfluidics could solve current problems in clinical diagnosis, such as eliminating intrinsic fluorescence background noise in clinical assays. The effects of mentioned factors during synthesis of MNPs and QDs and fabrication of MQDs and their *in vivo* or *in vitro* applications are yet to be fully explored. Biodegradability and removing MQDs from the body after the target aims and their allowed dosage in the body are additional key features that needs further investigation to address health and safety issues. Most of the MQDs are fabricated in laboratory scales, while their large scale synthesis and their stability for a long time is another important subject that need more investigations. Application of MQDs in biomedical sciences is imminent and expected to grow in coming years due to their multimodal functionality most useful for; (a) rapid point-of-care based nano-diagnostic systems, (b) form new classes of smart imaging and theranostic nanorobots, (c) magnetic heating and hyperthermia treatments and (d) drug delivery systems for their biological activity in personalized therapeutic applications.

Acknowledgements

This work was supported by the Scientific and Technological Research Council of Turkey (TÜBITAK) Grant No. 118Z460 and the authors thank for the support.

References

[1] M. Torkpur-Biglarianzadeh, M. Salami-Kalajahi, RSC Advances, 5 (2015) 29653-29662.

[2] K. Sato, E. Abe, M. Takahashi, J.-i. Anzai, Journal of Colloid and Interface Science, 432 (2014) 92-97.

[3] S. Wang, W. Yang, H. Du, F. Guo, H. Wang, J. Chang, X. Gong, B. Zhang, Nanotechnology, 27 (2016) 165101.

[4] K. Yan, H. Li, P. Li, H. Zhu, J. Shen, C. Yi, S. Wu, K.W.K. Yeung, Z. Xu, H. Xu, P.K. Chu, Biomaterials, 35 (2014) 344-355.

[5] E. Perillo, K. Hervé-Aubert, E. Allard-Vannier, A. Falanga, S. Galdiero, I. Chourpa, Journal of Colloid and Interface Science, 499 (2017) 209-217.

[6] B. Ullrich, J.S. Wang, X.Y. Xiao, G.J. Brown, Quantum Dots and Nanostructures: Synthesis, Characterization, and Modeling IX, International Society for Optics and Photonics, 2012, pp. 82710A.

[7] A. Armaselu, OPTOELECTRONICS AND ADVANCED MATERIALS-RAPID COMMUNICATIONS, 9 (2015) 531-536.

[8] J. Wang, S. Han, D. Ke, R. Wang, Journal of Nanomaterials, 2012 (2012) 1.

[9] V. Biju, S. Mundayoor, R.V. Omkumar, A. Anas, M. Ishikawa, Biotechnology Advances, 28 (2010) 199-213.

[10] E.İ. Altınoğlu, J.H. Adair, Wiley Interdisciplinary Reviews: Nanomedicine and Nanobiotechnology, 2 (2010) 461-477.

[11] J. Gao, K. Chen, R. Xie, J. Xie, Y. Yan, Z. Cheng, X. Peng, X. Chen, Bioconjugate Chemistry, 21 (2010) 604-609.

[12] A. Guchhait, A.K. Rath, A.J. Pal, Solar Energy Materials and Solar Cells, 95 (2011) 651-656.

[13] D.J. Bharali, D.W. Lucey, H. Jayakumar, H.E. Pudavar, P.N. Prasad, Journal of the American Chemical Society, 127 (2005) 11364-11371.

[14] Z. Chen, P. Li, Z. Zhang, X. Zhai, J. Liang, Q. Chen, K. Li, G. Lin, T. Liu, Y. Wu, Analytical Chemistry, 91 (2019) 5777-5785.

[15] X. Qiu, K.D. Wegner, Y.-T. Wu, P. M.P. van Bergen en Henegouwen, T.L. Jennings, N. Hildebrandt, Chemistry of Materials, 28 (2016) 8256-8267.

[16] C.M. Tyrakowski, P.T. Snee, Analytical Chemistry, 86 (2014) 2380-2386.

[17] R. Bakalova, Z. Zhelev, H. Ohba, Y. Baba, Journal of the American Chemical Society, 127 (2005) 9328-9329.

[18] R. Bilan, A. Ametzazurra, K. Brazhnik, S. Escorza, D. Fernández, M. Uríbarri, I. Nabiev, A. Sukhanova, Scientific Reports, 7 (2017) 44668.

[19] R.S. Bilan, V.A. Krivenkov, M.A. Berestovoy, A.E. Efimov, I.I. Agapov, P.S. Samokhvalov, I. Nabiev, A. Sukhanova, ChemPhysChem, 18 (2017) 970-979.

[20] L. Anfossi, F. Di Nardo, S. Cavalera, C. Giovannoli, G. Spano, E.S. Speranskaya, I.Y. Goryacheva, C. Baggiani, Microchimica Acta, 185 (2018) 94.

[21] Z. Lin, S. Lv, K. Zhang, D. Tang, Journal of Materials Chemistry B, 5 (2017) 826-833.

[22] Z. Qiu, J. Shu, D. Tang, Analytical Chemistry, 89 (2017) 5152-5160.

[23] M. Miyashita, K. Gonda, H. Tada, M. Watanabe, N. Kitamura, T. Kamei, H. Sasano, T. Ishida, N. Ohuchi, Cancer Medicine, 5 (2016) 2813-2824.

[24] S. Wang, W.M. Li, D.Z. Yuan, J.D. Song, J. Fang, Int J Nanomed, 11 (2016) 235-247.

[25] X.Q. Yang, C. Chen, C.W. Peng, J.X. Hou, S.P. Liu, C.B. Qi, Y.P. Gong, X.B. Zhu, D.W. Pang, Y. Li, Int J Nanomed, 6 (2011) 2265-2273.

[26] Z.L. Hu, G.Q. Qian, S. Muller, J. Xu, N.F. Saba, S.J. Kim, Z.J. Chen, N. Jiang, D.S. Wang, H.Z. Zhang, K. Lane, C. Hoyt, D.M. Shin, Z.G. Chen, Oncotarget, 7 (2016) 44676-44685.

[27] M. Hu, J. Yan, Y. He, H. Lu, L. Weng, S. Song, C. Fan, L. Wang, ACS Nano, 4 (2010) 488-494.

[28] L.-J. Zhang, L. Xia, H.-Y. Xie, Z.-L. Zhang, D.-W. Pang, Analytical Chemistry, 91 (2019) 532-547.

[29] H. Shen, A.M. Jawaid, P.T. Snee, ACS Nano, 3 (2009) 915-923.

[30] P.T. Snee, Accounts of Chemical Research, 51 (2018) 2949-2956.

[31] A.K. Gupta, M. Gupta, Biomaterials, 26 (2005) 3995-4021.

[32] K.D. Mahajan, Q. Fan, J. Dorcéna, G. Ruan, J.O. Winter, Biotechnology Journal, 8 (2013) 1424-1434.

[33] M. Makkar, R. Viswanatha, Current Science, 112 (2017) 1421.

[34] R. Kumar, K. Mondal, P.K. Panda, A. Kaushik, R. Abolhassani, R. Ahuja, H.G. Rubahn, Y.K. Mishra, J Mater Chem B, (2020).

[35] J.-S. Lee, M.I. Bodnarchuk, E.V. Shevchenko, D.V. Talapin, Journal of the American Chemical Society, 132 (2010) 6382-6391.

[36] S. Deng, G. Ruan, N. Han, J.O. Winter, Nanotechnology, 21 (2010) 145605.

[37] A.W. Lin, C.Y. Ang, P.K. Patra, Y. Han, H. Gu, J.-M. Le Breton, J. Juraszek, H. Chiron, G.C. Papaefthymiou, S.T. Selvan, Journal of Solid State Chemistry, 184 (2011) 2150-2158.

[38] S. Bhandari, R. Khandelia, U.N. Pan, A. Chattopadhyay, ACS applied materials & interfaces, 7 (2015) 17552-17557.

[39] L. Sun, Y. Zang, M. Sun, H. Wang, X. Zhu, S. Xu, Q. Yang, Y. Li, Y. Shan, Journal of colloid and interface science, 350 (2010) 90-98.

[40] Y. Xu, A. Karmakar, D. Wang, M.W. Mahmood, F. Watanabe, Y. Zhang, A. Fejleh, P. Fejleh, Z. Li, G. Kannarpady, The Journal of Physical Chemistry C, 114 (2010) 5020-5026.

[41] E. Song, W. Han, J. Li, Y. Jiang, D. Cheng, Y. Song, P. Zhang, W. Tan, Analytical chemistry, 86 (2014) 9434-9442.

[42] Q. Ma, Y. Nakane, Y. Mori, M. Hasegawa, Y. Yoshioka, T.M. Watanabe, K. Gonda, N. Ohuchi, T. Jin, Biomaterials, 33 (2012) 8486-8494.

[43] K. Wang, J. Ruan, Q. Qian, H. Song, C. Bao, X. Zhang, Y. Kong, C. Zhang, G. Hu, J. Ni, Journal of nanobiotechnology, 9 (2011) 23.

[44] K. Koc, B. Karakus, K. Rajar, E. Alveroglu, Superlattices and Microstructures, 110 (2017) 198-204.
[45] N. Yin, P. Wu, G. Liang, W. Cheng, Applied Physics A, 122 (2016) 243.
[46] R. Gui, Y. Wang, J. Sun, Colloids and Surfaces B: Biointerfaces, 113 (2014) 1-9.
[47] N.Ž. Knežević, V.S.-Y. Lin, Nanoscale, 5 (2013) 1544-1551.
[48] Z. Wang, X. Jiang, W. Liu, G. Lu, X. Huang, Science China Chemistry, 62 (2019) 889-896.
[49] Y. Qiu, R. Palankar, M. Echeverría, N. Medvedev, S.E. Moya, M. Delcea, Nanoscale, 5 (2013) 12624-12632.
[50] J.-C. Hsu, C.-C. Huang, K.-L. Ou, N. Lu, F.-D. Mai, J.-K. Chen, J.-Y. Chang, Journal of Materials Chemistry, 21 (2011) 19257-19266.
[51] Y.-H. Li, T. Song, J.-Q. Liu, S.-J. Zhu, J. Chang, Journal of Materials Chemistry, 21 (2011) 12520-12528.
[52] Y.F. Tan, P. Chandrasekharan, D. Maity, C.X. Yong, K.-H. Chuang, Y. Zhao, S. Wang, J. Ding, S.-S. Feng, Biomaterials, 32 (2011) 2969-2978.
[53] D.H. Ortgies, L. de la Cueva, B. del Rosal, F. Sanz-Rodríguez, N. Fernández, M.C. Iglesias-de la Cruz, G. Salas, D. Cabrera, F.J. Teran, D. Jaque, ACS applied materials & interfaces, 8 (2016) 1406-1414.
[54] L. Lou, K. Yu, Z. Zhang, B. Li, J. Zhu, Y. Wang, R. Huang, Z. Zhu, Nanoscale, 3 (2011) 2315-2323.
[55] D. Koktysh, V. Bright, W. Pham, Nanotechnology, 22 (2011) 275606.
[56] B. Chen, H. Zhang, C. Zhai, N. Du, C. Sun, J. Xue, D. Yang, H. Huang, B. Zhang, Q. Xie, Journal of Materials Chemistry, 20 (2010) 9895-9902.
[57] L. Liu, L. Xiao, H.-Y. Zhu, Chemical Physics Letters, 539 (2012) 112-117.
[58] S.R. Ahmed, J. Dong, M. Yuki, T. Kato, J. Lee, E.Y. Park, Journal of nanobiotechnology, 11 (2013) 28.
[59] I. Hocaoglu, D. Asik, G. Ulusoy, C. Grandfils, I. Ojea-Jimenez, F. Rossi, A. Kiraz, N. Doğan, H.Y. Acar, Colloids and Surfaces B: Biointerfaces, 133 (2015) 198-207.
[60] Z. Li, G. Wang, Y. Shen, N. Guo, N. Ma, Advanced Functional Materials, 28 (2018) 1707152.
[61] G. Ruan, G. Vieira, T. Henighan, A. Chen, D. Thakur, R. Sooryakumar, J.O. Winter, Nano letters, 10 (2010) 2220-2224.
[62] X. Sun, K. Ding, Y. Hou, Z. Gao, W. Yang, L. Jing, M. Gao, The Journal of Physical Chemistry C, 117 (2013) 21014-21020.
[63] V.G. Demillo, M. Liao, X. Zhu, D. Redelman, N.G. Publicover, K.W. Hunter Jr, Colloids and Surfaces A: Physicochemical and Engineering Aspects, 464 (2015) 134-142.
[64] W.-S. Zou, J. Yang, T.-T. Yang, X. Hu, H.-Z. Lian, Journal of Materials Chemistry, 22 (2012) 4720-4727.

[65] H.-S. Cho, Z. Dong, G.M. Pauletti, J. Zhang, H. Xu, H. Gu, L. Wang, R.C. Ewing, C. Huth, F. Wang, ACS nano, 4 (2010) 5398-5404.

[66] S. Walia, S. Sharma, P.M. Kulurkar, V. Patial, A. Acharya, International journal of pharmaceutics, 498 (2016) 110-118.

[67] Y. Ding, H. Yin, S. Shen, K. Sun, F. Liu, New Journal of Chemistry, 41 (2017) 1736-1743.

[68] F.-Y. Cheng, C.-H. Su, P.-C. Wu, C.-S. Yeh, Chemical communications, 46 (2010) 3167-3169.

[69] S.N. Yin, C.F. Wang, Z.Y. Yu, J. Wang, S.S. Liu, S. Chen, Advanced materials, 23 (2011) 2915-2919.

[70] H.-M. Fan, M. Olivo, B. Shuter, J.-B. Yi, R. Bhuvaneswari, H.-R. Tan, G.-C. Xing, C.-T. Ng, L. Liu, S.S. Lucky, Journal of the American Chemical Society, 132 (2010) 14803-14811.

[71] E.S. Shibu, K. Ono, S. Sugino, A. Nishioka, A. Yasuda, Y. Shigeri, S.-i. Wakida, M. Sawada, V. Biju, ACS nano, 7 (2013) 9851-9859.

[72] I.V. Martynenko, D. Kusic, F. Weigert, S. Stafford, F.C. Donnelly, R. Evstigneev, Y. Gromova, A.V. Baranov, B. Rühle, H.-J.r. Kunte, Analytical chemistry, 91 (2019) 12661-12669.

[73] A. Qureshi, A. Tufani, G. Corapcioglu, J.H. Niazi, Sensors and Actuators B: Chemical, (2020) 128431.

[74] A. Saha, A. Shetty, A. Pavan, S. Chattopadhyay, T. Shibata, R. Viswanatha, The journal of physical chemistry letters, 7 (2016) 2420-2428.

[75] X. Liu, H. Jiang, J. Ye, C. Zhao, S. Gao, C. Wu, C. Li, J. Li, X. Wang, Advanced functional materials, 26 (2016) 8694-8706.

[76] C.-L. Li, B.-R. Huang, J.-Y. Chang, J.-K. Chen, Journal of Materials Chemistry C, 3 (2015) 4603-4615.

Declaration of competing interest

The authors declare that they have no known competing financial interests or personal relationships that could have appeared to influence the work reported in this paper.

Graphical abstract

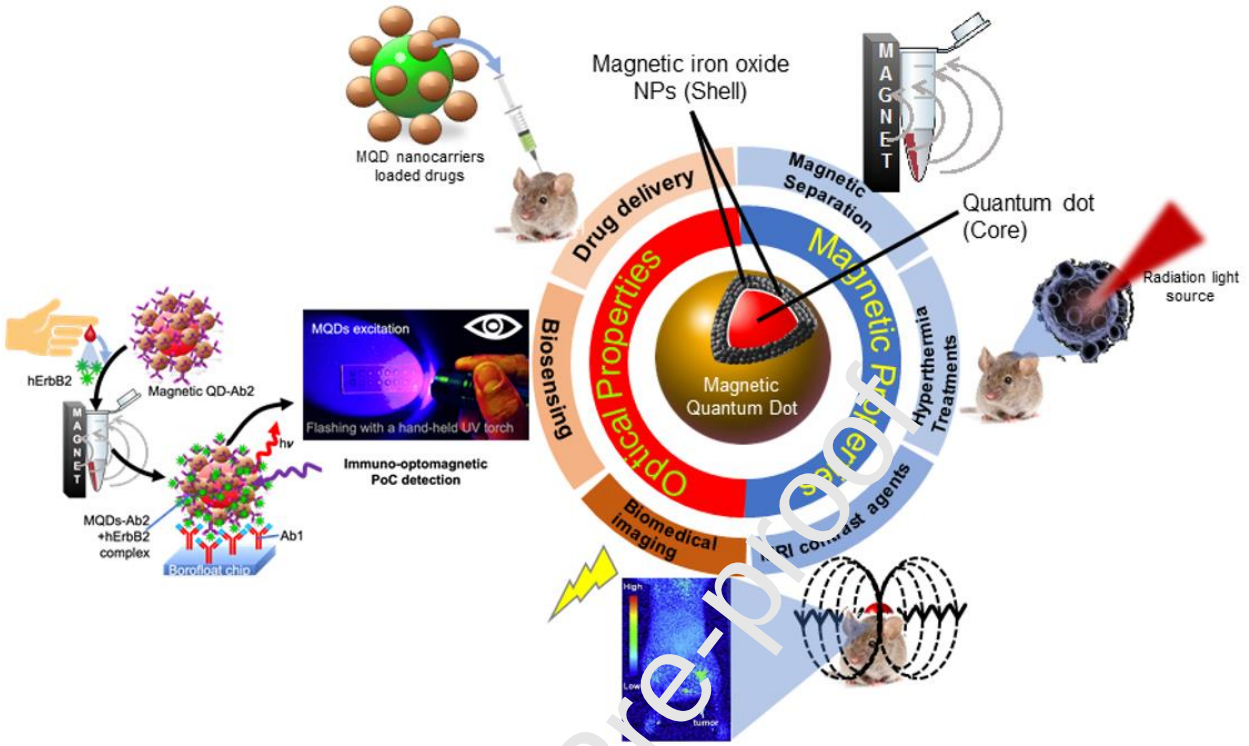

Highlights

(a) Recent strategies for chemical synthesis and integration of magnetic iron oxide nanoparticles and luminescent quantum dots.

(b) Multifunctional magnetic luminescent quantum dots (MQDs) that has been used for biological, biomedical or diagnostic applications, such as magnetic resonance imaging (MRI), point of care based diseases nano-diagnostic, theranostics nanorobots and other bio-medical applications.

(c) Future prospects of MQDs are addressed.